

# High Dielectric Constant Semiconducting Poly(3-alkylthiophene)s from Side Chain Modification with Polar Sulfinyl and Sulfonyl Groups

C. Wang, R. Li

To be published in "MACROMOLECULES"

November 2018

Photon Sciences

**Brookhaven National Laboratory**

**U.S. Department of Energy**

USDOE Office of Science (SC), Basic Energy Sciences (BES) (SC-22)

Notice: This manuscript has been authored by employees of Brookhaven Science Associates, LLC under Contract No. DE-SC0012704 with the U.S. Department of Energy. The publisher by accepting the manuscript for publication acknowledges that the United States Government retains a non-exclusive, paid-up, irrevocable, world-wide license to publish or reproduce the published form of this manuscript, or allow others to do so, for United States Government purposes.

## **DISCLAIMER**

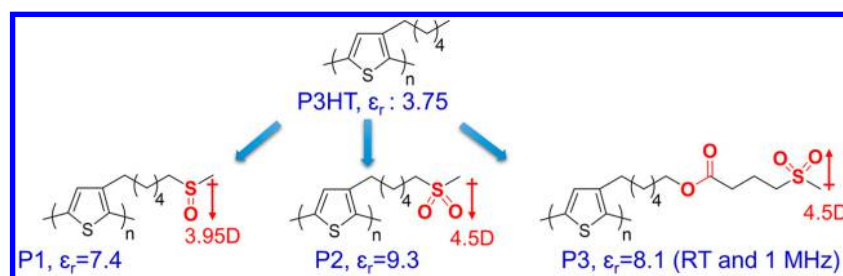
This report was prepared as an account of work sponsored by an agency of the United States Government. Neither the United States Government nor any agency thereof, nor any of their employees, nor any of their contractors, subcontractors, or their employees, makes any warranty, express or implied, or assumes any legal liability or responsibility for the accuracy, completeness, or any third party's use or the results of such use of any information, apparatus, product, or process disclosed, or represents that its use would not infringe privately owned rights. Reference herein to any specific commercial product, process, or service by trade name, trademark, manufacturer, or otherwise, does not necessarily constitute or imply its endorsement, recommendation, or favoring by the United States Government or any agency thereof or its contractors or subcontractors. The views and opinions of authors expressed herein do not necessarily state or reflect those of the United States Government or any agency thereof.

# High Dielectric Constant Semiconducting Poly(3-alkylthiophene)s from Side Chain Modification with Polar Sulfinyl and Sulfonyl Groups

Chunlai Wang,<sup>†</sup> Zhongbo Zhang,<sup>†,‡</sup> Sandra Pejić,<sup>†</sup> Ruipeng Li,<sup>§</sup> Masafumi Fukuto,<sup>§</sup> Lei Zhu,<sup>\*,†,‡</sup> and Geneviève Sauvé<sup>\*,†</sup>

<sup>†</sup>Department of Chemistry and <sup>‡</sup>Department of Macromolecular Science and Engineering, Case Western Reserve University, Cleveland, Ohio 44106, United States

<sup>§</sup>National Synchrotron Light Source II, Brookhaven National Laboratory, Upton, New York 11973, United States



**ABSTRACT:** There is growing interest in designing and developing high dielectric constant ( $\epsilon_r$ ) organic semiconductors because they have the potential to further enhance device performance by promoting exciton dissociation, reducing bimolecular charge carrier recombination, and potentially enhancing charge carrier mobility via charge screening. In this study, a new class of semiconducting polymers with high  $\epsilon_r$ , i.e., sulfinylated and sulfonylated poly(3-alkylthiophene)s (P3ATs), were synthesized. Because of efficient rotation of highly polar methylsulfinyl and methylsulfonyl side groups (i.e., orientational polarization), high  $\epsilon_r$  values were achieved for these functionalized P3ATs based on an accurate capacitance measurement using a gold/semiconducting polymer/SiO<sub>2</sub>/n-doped Si configuration. For example, the  $\epsilon_r$  at megahertz and room temperature increased from 3.75 for the regioregular poly(3-hexylthiophene) (P3HT) to 7.4 for the sulfinylated and 8.1–9.3 for sulfonylated P3AT polymers. These values are among the highest  $\epsilon_r$  reported for conjugated polymers so far. Grazing-incident wide-angle X-ray diffraction results showed that these polar groups decreased the crystallinity for the polythiophene backbones and interfered with the  $\pi$ - $\pi$  stacking in the crystalline structure. Consequently, their optical properties, including UV-vis absorption and fluorescence, changed in thin films. From this study, the sulfinylated polymer may be promising to provide a balance between high  $\epsilon_r$  and preserving favorable polythiophene  $\pi$ - $\pi$  stacking structure for device applications.

## INTRODUCTION

Organic semiconductors have attracted much attention due to their potential use in electronic applications. Most research efforts have been dedicated to the optimization of semiconductors' optical, electrochemical, electrical, and structural properties. A much less investigated property of organic semiconductors is the relative permittivity or dielectric constant ( $\epsilon_r$ ) and its effect on optoelectronic properties and device performance. Organic semiconductors typically have a low  $\epsilon_r$ , only 3–4, as compared to inorganic semiconductors; e.g.,  $\epsilon_r$  for Si is  $\sim 11$ .

High  $\epsilon_r$  semiconductors in inorganic solar cells and lead halide perovskite solar cells all have low exciton binding energy, such as Si (15 meV), GaN (20 meV), and CH<sub>3</sub>NH<sub>3</sub>PbI<sub>3</sub> (10 meV). These excitons can easily split into free charge carriers by thermal energy  $k_B T$  (i.e., around 25 meV at room temperature) for efficient device performance.<sup>1,2</sup> This could be largely attributed to their high dielectric constants at

high frequencies. For example, the  $\epsilon_r$  of lead halide perovskites at terahertz frequencies is about 20–28.<sup>3–6</sup> However, excitons generated in most organic semiconductors have an exciton energy of at least 100 meV.<sup>7–10</sup> To overcome this large energy barrier to dissociate excitons, a heterojunction architecture composed of a donor and an acceptor with proper energy level offsets must be used. Nonetheless, these energy offsets lead to a decrease in the open circuit voltage ( $V_{oc}$ ) and thereby limit the overall device performance. The dissociation probability of excitons in inorganic semiconductors such as Si is about 2 orders of magnitude higher than that in organic semiconductors.<sup>11</sup> Koster et al. predicted that exciton binding energies of organic semiconductors could be reduced to the order of  $k_B T$ , if the  $\epsilon_r$  of organic semiconductors can be

increased to  $\sim 10$ .<sup>12</sup> This would enable a homojunction organic photovoltaics (OPVs) with a single photoactive material. Moreover, a number of authors have argued that the strength of charge screening is one of the most contributing factors to charge dissociation in OPVs, and high  $\epsilon_r$  organic semiconductors can effectively suppress charge recombination.<sup>12–14</sup>

Increasing  $\epsilon_r$  can be realized through enhancing various polarizations, including electronic, atomic/vibrational, and orientational/dipolar polarizations.<sup>15</sup> Before exploring viable approaches, it is desirable to understand the opportunities in enhancing different polarizations for polymers. First, one could utilize space charges, which include both electron/holes and ionic species. However, polarization (or conduction) of electrons and holes will not increase the capacitance and thus the  $\epsilon_r$  of a semiconducting polymer. Interfacial polarization (or conduction) of ionic species will increase the overall capacitance (through the electric double layer, EDL) but not the genuine  $\epsilon_r$  of a dielectric polymer.<sup>16</sup> Therefore, space charge polarization should not be utilized to enhance  $\epsilon_r$  for conjugated polymers. In contrast, atomic and electronic polarizations improve  $\epsilon_r$  at very high frequency (above terahertz) and could potentially reduce exciton binding energy as well as charge transfer exciton attraction. However, the  $\epsilon_r$  enhancement from atomic and electronic polarizations has been limited between 2 and 5 due to the nature of covalent bonds for organic polymers, and there is an inverse upper-limit relationship between the bandgap and  $\epsilon_r$ .<sup>15,17,18</sup> We recently tested an idea that utilizes the keto–enol tautomeric structures in fluorescein monopotassium salt-containing side-chain semiconducting polymers to enhance the  $\epsilon_r$ .<sup>19</sup> A relatively high  $\epsilon_r$  of 5.5 was achieved at high frequencies, which is promising in promoting charge carrier mobility in the solid state.

Alternatively, orientational or dipolar polarization, which originates from rotation of dipolar groups, can be utilized to further enhance the  $\epsilon_r$  of polymers. Dipolar polarization happens at frequencies below  $10^{10}$  Hz, which is at the same time scale for most bimolecular recombination in organic semiconductors. An enhancement of dielectric constant and device performance could also be achieved by blending a high-permittivity small molecule with the semiconducting polymer.<sup>20</sup> However, it was difficult to achieve high dielectric constants because of the macrophase separation of the small molecules at high concentrations. As a result of macrophase separation, the dielectric constant will decrease as well as the device performance. Instead, side chain functionalization with polar groups has been shown to be a practical method for improving  $\epsilon_r$  of organic semiconductors without deteriorating other parameters such as crystalline morphology and charge mobility.<sup>13</sup> de Gier et al. demonstrated that increasing  $\epsilon_r$  of organic semiconductors with dipolar polarization can lower the Coulombic attraction between electrons and holes in the charge transfer state, if the polar groups can rotate fast enough in the solid films under the applied field.<sup>21</sup>

Yang et al. showed that adding fluorine substituents on the backbone of a conjugated polymer (P0F) increased the  $\epsilon_r$  from 6.6 to 7.2 for P1F with one fluorine per repeat unit and then to 7.9 for P2F with two fluorines per repeat unit. When blended with PCBM in devices, both P1F and P2F exhibited decreased charge transfer exciton energy and improved  $V_{oc}$  when compared with P0F.<sup>22</sup> Cho et al. demonstrated that increasing the  $\epsilon_r$  of PIDT-DPP-alkyl (i.e., indacenodithiophene-based copolymer containing diketopyrrolopyrrole unit with alkyl chains) from 3.5 to 5.0 by incorporating highly polar nitrile

groups on the side chains improved both charge carrier lifetime and device performance in a bilayer device.<sup>23</sup> Armin et al. synthesized a dimer and a polymer by substituting the alkyl side chain of DA (i.e., a dimer of 2-((7-(4,4-di-*n*-octyl-4*H*-cyclopenta[2,1-*b*:3,4-*b'*])dithiophen-2-yl)benzo[*c*][1,2,5]-thiadiazol-4-yl)methylene)malononitrile) and PCPDTBT (i.e., poly[2,6-(4,4-bis{2-ethylhexyl}-4*H*-cyclopenta[2,1-*b*:3,4-*b'*]-dithiophene)-*alt*-4,7-(2,1,3-benzothiadiazole)]) with polarizable oligo(ethylene glycol) side chains.<sup>24</sup> As a result, the  $\epsilon_r$  increased from 3.6 up to 6.1 at low frequencies. Homojunction quantum efficiencies of glycolated materials were also improved compared with the alkylated analogues.

Although some progress has been made to improve  $\epsilon_r$  of organic semiconductors via side chain modification, the  $\epsilon_r$  values are still limited to around 6 for conjugated polymers. Because dipolar polarization is proportional to the square of dipole moment ( $\mu$ ) for polar molecules,<sup>25</sup> functional groups with a high  $\mu$  can induce a larger polarization. These high  $\mu$  groups include nitrate  $-\text{NO}_2$  ( $\sim 3.6$  D), nitrile  $-\text{CN}$  ( $\sim 3.95$  D), sulfinyl  $-\text{SO}-$  ( $\sim 3.96$  D), and sulfonyl  $-\text{SO}_2-$  ( $\sim 4.5$  D) groups. The sulfonyl group has been proved to be a good candidate for enhancing  $\epsilon_r$  of dipolar glass polymers. For example, it was demonstrated that the  $\epsilon_r$  of poly[2-(methylsulfonyl)ethyl methacrylate] (PMSEMA) can reach 11–12 at room temperature (i.e., below its glass transition temperature,  $T_g \sim 110$  °C), which is nearly 3 times that of its analogue polymer, poly(methyl methacrylate) (PMMA).<sup>26</sup> Later, other sulfonyl-containing polymers were also synthesized, and they exhibited enhanced  $\epsilon_r$  below the  $T_g$  due to enhanced dipolar polarization from facile rotation of sulfonyl side groups.<sup>27,28</sup>

In this study, we intend to increase  $\epsilon_r$  of semiconducting regioregular poly(3-alkylthiophene)s by implementing methylsulfinyl or methylsulfonyl groups at the ends of the alkyl side chains. The effect of end-group functionalization on the crystalline structure of polythiophene backbones is studied by differential scanning calorimetry (DSC) and grazing-incident wide-angle X-ray diffraction (GI-WAXD). The  $\pi$ – $\pi$  interaction and crystallinity of polythiophene backbones appear to be affected by the strong interaction among polar sulfinyl and sulfonyl end groups. As a result, the optical properties (i.e., UV–vis absorption and fluorescence) in thin films are altered compared to neat P3HT. A new dielectric characterization method utilizing the metal/semiconducting polymer/SiO<sub>2</sub>/*n*-doped Si (MPOS) sample geometry is proposed to accurately determine the  $\epsilon_r$  of semiconducting polymers without any interference from space charge conduction. Broadband dielectric spectroscopy (BDS) results show that the  $\epsilon_r$  values increase from 3.75 for neat P3HT to 7.4–9.3 for functionalized P3AT polymers at 1 MHz and room temperature. Preliminary BDS results suggest that the charge carrier mobilities in these functionalized P3AT polymers are higher than that in neat P3HT. On the basis of these initial characterization results, we plan to study device performance for these high  $\epsilon_r$  polymers in the future.

## ■ EXPERIMENTAL SECTION

**Materials.** Tetrahydrofuran (THF) was freshly distilled over CaH<sub>2</sub> and stored in a refrigerator before use. Anhydrous *N,N*-dimethylformamide (DMF) was purchased from Fisher Scientific. 2,5-Dibromo-3-hexylthiophene and 2,5-dibromo-3-(6-bromohexyl)-thiophene were synthesized according to a published procedure.<sup>29</sup> *m*-Chloroperoxybenzoic acid (*m*-CPBA) was purchased from Sigma-

Aldrich and was further purified according to a published procedure.<sup>30</sup> All other chemicals were purchased from either Sigma-Aldrich or Fisher Scientific and used as received.

#### General Characterization Methods and Instrumentation.

Proton nuclear magnetic spectroscopy (<sup>1</sup>H NMR) spectra were recorded using a 500 MHz Bruker Ascend Advance III High Definition (HD). The chemical shift for <sup>1</sup>H NMR was reported in parts per million (ppm) relative to tetramethylsilane, Si(CH<sub>3</sub>)<sub>4</sub>. Matrix-assisted laser desorption/ionization time-of-flight (MALDI-TOF) mass spectra (MS) were measured on a Bruker Autoflex III MALDI-TOF mass spectrometer, and samples were prepared from chloroform solutions using a terthiophene matrix. Molecular weight distribution (or polydispersity, PDI) was estimated from weight ( $M_w$ ) and number-average molecular weights ( $M_n$ , PDI =  $M_w/M_n$ ) determined by size-exclusion chromatography (SEC) using a Tosoh HPLC-8320. The system was operated at a flow rate of 0.35 mL/min and 25 °C using HPLC grade THF as eluent and calibrated using linear polystyrene (PS) standards. Elemental analyses (C, H, and S) were performed under optimum combustion conditions by Robertson Microlit Laboratories (Ledgewood, NJ).

UV-vis absorption spectra were collected on a Cary 50 UV-vis spectrometer. Fluorescence spectra were collected on a Cary Eclipse fluorescence spectrophotometer. The excitation wavelengths for solutions and films were 450 and 550 nm, respectively. All solutions were made using chloroform with 6 vol % methanol. All films were prepared from a 10 mg/mL solution in chloroform with 6 vol % methanol. The solution was filtered through a 0.45 μm PTFE filter and then spin-coated at 800 rpm for 60 s. All films were annealed at 150 °C for 10 min before measurement.

Thin film cyclic voltammetry (CV) measurements were performed at room temperature using an Autolab PGSTAT 302N Exo Chemie potentiostat. CV measurements were performed using 0.1 M Bu<sub>4</sub>NPF<sub>6</sub> in dry acetonitrile or DMF as the electrolyte solution and ferrocene/ferrocenium (Fc/Fc<sup>+</sup>) as the internal standard. The solution was purged with nitrogen for 15 min prior to the measurement. An Ag/AgNO<sub>3</sub> electrode was used as the reference electrode ( $E_{1/2} = 0.091$  V vs Fc/Fc<sup>+</sup>), a Pt wire was used as the counter electrode, and a polished glassy carbon (GC) electrode served as the working electrode. Films were cast from the 10 mg/mL solution in chloroform with 6 vol % methanol, which was filtered through a 0.45 μm PTFE filter. For CV measurement in solution, 5 mg of compound (R-P3 and P2) were fully dissolved in the electrolyte solution before measurement. All scans were performed at a scan rate of 0.1 V/s. The highest occupied molecular orbital (HOMO) energy levels were estimated from the onsets of the oxidation potential, and a value of 5.1 eV vs vacuum was used for Fc/Fc<sup>+</sup>, i.e., HOMO =  $-(E_{\text{onset,ox}} + 5.1)$  eV.

Thermal gravimetric analysis (TGA) was performed on a TA Instruments Q500 thermogravimetric analyzer. Weight loss was recorded by heating the sample from 25 to 800 °C at a heating scan rate of 20 °C/min. DSC was performed on a TA Instruments Q2000 differential scanning calorimeter with a scanning rate of 10 °C/min up to 300 °C.

Dielectric constants of semiconducting polymers were characterized using a gold/semiconducting polymer/SiO<sub>2</sub>/n-doped Si configuration. Polymer films were cast on the SiO<sub>2</sub> surface from different solutions with a concentration of 20 mg/mL; P3HT in *o*-dichlorobenzene, P1 in 1:1 (vol/vol) dichloromethane and DMF, and P2 and P3 in DMF. With an optimized solvent evaporation process, the polymer film thickness had a standard deviation of 10–15%. Gold electrodes of 2.4 mm in diameter and ~10 nm in thickness were evaporated on the top surface of the polymer films for broadband dielectric spectroscopy (BDS) characterization. Capacitance measurements were performed on a Novocontrol Concept 80 broadband dielectric spectrometer with frequency from 1 to 10<sup>6</sup> Hz and temperature from –50 to 75 °C at 1.0 V<sub>rms</sub> (i.e., root-mean-square voltage).

Tapping-mode atomic force microscopy (AFM) was performed on polymer films using a Bruker Veeco Digital Instrument 3100 microscope and a Nanoscope controller. AFM images were analyzed

by Windows Application for Data Processing in Scanning Probe Microscopy (WSxM 5.0) Develop 8.0.

GI-WAXD measurements were performed using the 11-BM Complex Materials Scattering (CMS) beamline at the National Synchrotron Light Source II (NSLS-II), Brookhaven National Laboratory. The monochromatized X-ray wavelength was  $\lambda = 0.0918$  nm. An in-vacuum CCD detector (Photonic Science) was used to collect GI-WAXD patterns. The polymer films were illuminated by the collimated X-ray beam at an incidence angle of about 0.1°. The distance between the sample and the detector was 222.2 mm, which was calibrated using silver behenate with the first-order reflection at a scattering vector of  $q = 1.076$  nm<sup>-1</sup>. The data acquisition time for each GI-WAXD pattern was 10 s. Polar Brook Technology and Applied Research, Inc., Stony Brook, NY software was used for data analysis.

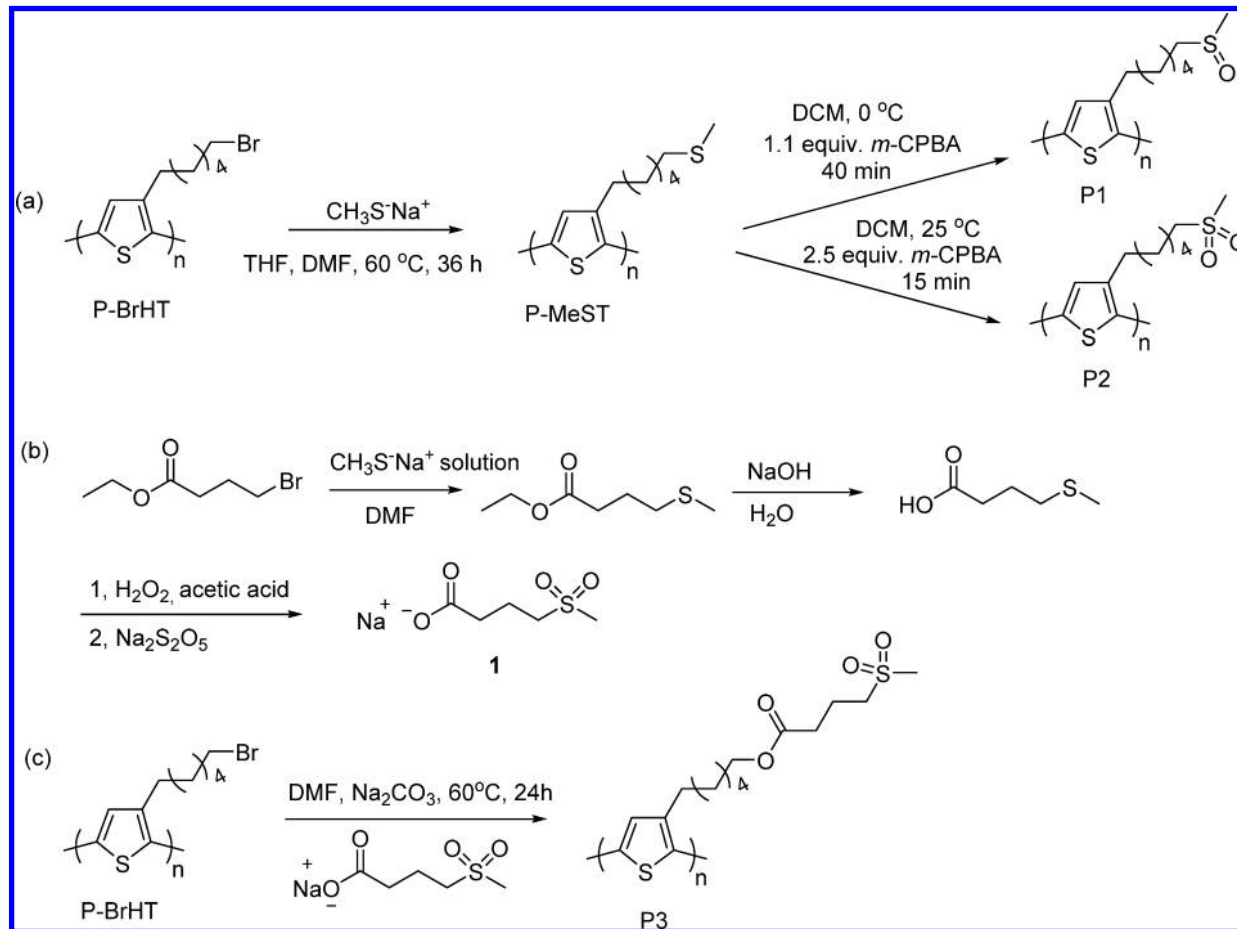
**Monomer and Polymer Syntheses.** *Sodium 4-(Methylsulfonyl)butanoate (1)*. Ethyl 4-bromobutanoate (15 mL, 0.1 mol), and 50 mL of sodium thiomethoxide solution (20 wt %, 0.12 mol), and 90 mL of DMF were added into a 500 mL one-neck round-bottom flask, and the mixture was stirred at 25 °C for 48 h. The reaction was quenched with 60 mL cold water and then was extracted three times with diethyl ether, washed one time with brine, dried with anhydrous magnesium sulfate, filtered through filter paper, and evaporated to obtain a colorless oil product, ethyl 4-(methylthio)butanoate, 5.1 g (31.4 mmol, 31% isolated yield). <sup>1</sup>H NMR (500 MHz, CDCl<sub>3</sub>,  $\delta$ ): 4.14 (q,  $J = 7.1$  Hz, –COOCH<sub>2</sub>–, 2H), 2.54 (t,  $J = 7.2$  Hz, –SCH<sub>2</sub>–, 2H), 2.43 (dd,  $J = 7.9$  Hz, –OOCCH<sub>2</sub>–, 2H), 2.10 (s, –SCH<sub>3</sub>, 3H), 1.93 (p,  $J = 7.3$  Hz, –SCH<sub>2</sub>CH<sub>2</sub>–, 2H), 1.26 (t,  $J = 7.1$  Hz, –OOCCH<sub>2</sub>CH<sub>3</sub>, 3H) (Figure S1). Ethyl 4-(methylthio)butanoate (2 g, 12.33 mmol) and 2.5 mL of ethanol were added into 25 mL of 2 M NaOH solution and stirred at 40 °C for 12 h. The reaction was cooled using an ice bath and then neutralized with hydrochloric acid. The mixture was then extracted three times with diethyl ether, washed with brine, dried with anhydrous magnesium sulfate, filtered through filter paper, and evaporated to obtain a colorless oil product, 4-(methylthio)butanoic acid, 1.37 g (10.2 mmol, 83% isolated yield). <sup>1</sup>H NMR (500 MHz, CDCl<sub>3</sub>,  $\delta$ ): 2.57 (t,  $J = 7.1$  Hz, –SCH<sub>2</sub>–, 2H), 2.52 (t,  $J = 7.3$  Hz, HOOCCH<sub>2</sub>–, 2H), 2.11 (s, –SCH<sub>3</sub>, 3H), 1.95 (p,  $J = 7.2$  Hz, –SCH<sub>2</sub>CH<sub>2</sub>–, 2H) (Figure S2). 4-(Methylthio)butanoic acid (1.37 g, 10.2 mmol) and 10 mL of acetic acid were added into 50 mL one-neck round-bottom flask, and 1.2 mL of hydroperoxide solution (30 wt %, 10 mmol) was added dropwise into the reaction and stirred at 25 °C for 1 h. Then, 2.4 mL of hydroperoxide solution (30 wt %, 20 mmol) was added dropwise into the reaction and stirred at 60 °C for 4 h. The reaction was quenched by adding sodium metabisulfite (0.76 g, 4 mmol), and acetic acid and water were evaporated to obtain a white solid, sodium 4-(methylsulfonyl)butanoate (1), 1.2 g (6.4 mmol, 64% isolated yield). <sup>1</sup>H NMR (500 MHz, CDCl<sub>3</sub>,  $\delta$ ): 3.12–3.18 (m, –SO<sub>2</sub>CH<sub>2</sub>–, 2H), 2.95 (s, –SO<sub>2</sub>CH<sub>3</sub>, 3H), 2.37 (dd,  $J = 9.37$  Hz, –OOCCH<sub>2</sub>–, 2H), 2.01–2.10 (m, –SO<sub>2</sub>CH<sub>2</sub>CH<sub>2</sub>–, 2H) (Figure S3).

*Regioregular Poly(3-hexylthiophene) (P3HT)*. P3HT was synthesized by the Grignard metathesis (or GRIM) method,<sup>31</sup> 0.5 g (33% yield). <sup>1</sup>H NMR (500 MHz, CDCl<sub>3</sub>,  $\delta$ ): 6.96 (s, =CH–, 1H), 2.68–2.85 (m, –ArCH<sub>2</sub>CH<sub>2</sub>CH<sub>2</sub>–, 2H), 1.61–1.75 (m, –ArCH<sub>2</sub>CH<sub>2</sub>CH<sub>2</sub>–, 2H), 1.37–1.74 (m, –ArCH<sub>2</sub>CH<sub>2</sub>CH<sub>2</sub>–, 2H), 1.27–1.36 (m, –CH<sub>2</sub>CH<sub>2</sub>CH<sub>3</sub>, 4H), 0.85–0.94 (m, –CH<sub>3</sub>, 3H) (Figure S4). SEC:  $M_n = 9900$  g mol<sup>-1</sup> and PDI = 1.30.

*Regioregular Poly[3-(6-bromohexyl)thiophene] (P-BrHT)*. P-BrHT was synthesized according to the literature procedure,<sup>29,32</sup> 0.58 g (46.4% yield). <sup>1</sup>H NMR (500 MHz, CDCl<sub>3</sub>,  $\delta$ ): 6.96 (s, =CH–, 1H), 3.41 (t,  $J = 6.4$  Hz, BrCH<sub>2</sub>CH<sub>2</sub>–, 2H), 2.72–2.87 (m, –ArCH<sub>2</sub>CH<sub>2</sub>CH<sub>2</sub>–, 2H), 1.87 (t,  $J = 6.5$  Hz, BrCH<sub>2</sub>CH<sub>2</sub>–, 2H), 1.63–1.78 (m, –ArCH<sub>2</sub>CH<sub>2</sub>CH<sub>2</sub>–, 2H), 1.39–1.55 (m, BrCH<sub>2</sub>CH<sub>2</sub>CH<sub>2</sub>CH<sub>2</sub>–, 4H) (Figure S5). SEC:  $M_n = 10800$  g mol<sup>-1</sup> and PDI = 1.28. MALDI-TOF MS for P-BrHT is shown in Figure S10.

*Poly[3-(6-methylthiohexyl)thiophene] (P-MeST)*. P-BrHT (0.2 g) and sodium thiomethoxide (0.23 g, 3.3 mmol) were added to a 50 mL one-neck round-bottom flask, which was vacuumed and purged with

Scheme 1. (a) Synthesis of Poly[3-(6-methylsulfinylhexyl)thiophene] (P1) and Poly[3-(6-methylsulfonylhexyl)thiophene] (P2); (b) Synthesis of Sodium 4-(Methylsulfonyl)butanoate (1); (c) Synthesis of Poly[3-(6-(3-methylsulfonylpropylcarbonyloxy)hexyl)thiophene] (P3)



dry  $N_2$  three times. Dry THF (16 mL) and anhydrous DMF (18 mL) were added to the flask using syringes and stirred at 50 °C under a  $N_2$  atmosphere for 36 h. The reaction was cooled to room temperature and poured into methanol to precipitate the product. The precipitate was collected into a Soxhlet thimble and extracted with methanol and chloroform. The product was collected from the chloroform fraction. After evaporating chloroform, the product was obtained as a dark green solid film (0.15 g, 86% isolated yield).  $^1H$  NMR (500 MHz,  $CDCl_3$ ,  $\delta$ ): 6.96 (s, =CH-, 1H), 2.71–2.85 (m,  $-ArCH_2CH_2CH_2-$ , 2H), 2.43–2.53 (m,  $-SCH_2-$ , 2H), 2.07 (s,  $-SCH_3$ , 3H), 1.68–1.76 (m,  $-ArCH_2CH_2CH_2-$ , 2H), 1.57–1.66 (m,  $-SCH_2CH_2-$ , 2H), 1.38–1.51 (m,  $-SCH_2CH_2CH_2CH_2-$ , 4H) (Figure S6).

**Poly[3-(6-methylsulfinylhexyl)thiophene] (P1).**<sup>33</sup> P-MeST (0.15 g) was dissolved in 20 mL of dichloromethane in a 50 mL one-neck round-bottom flask and stirred at 0 °C. Purified *m*-CPBA (0.13 g, 0.7 mmol) was dissolved in 2 mL of dichloromethane, and the solution was added dropwise into the flask in 10 min. After stirring at 0 °C for 30 min, the reaction was poured into diethyl ether to precipitate the product. The precipitate was collected into a Soxhlet thimble and extracted with diethyl ether and chloroform. The product was collected from the chloroform fraction. After evaporating chloroform, P1 was obtained as a dark green solid film (70 mg, 51% isolated yield).  $^1H$  NMR (500 MHz,  $CDCl_3$ ,  $\delta$ ): 6.95 (s, =CH-, 1H), 2.80 (t,  $-ArCH_2-$ , 2H), 2.59–2.74 (m,  $-SOCH_2-$ , 2H), 2.53 (s,  $-SOCH_3$ , 3H), 1.73–1.83 (m,  $-ArCH_2CH_2-$ , 2H), 1.64–1.74 (m,  $-SOCH_2-CH_2-$ , 2H), 1.39–1.56 (m,  $-SOCH_2CH_2CH_2CH_2-$ , 4H) (Figure S7). Elemental analysis: Calcd for  $(C_{11}H_{16}OS_2)_n$ : C 56.53%; H 6.91%; S 27.44%. Found: C 56.45%; H 7.09%; S 25.93%. MALDI-TOF MS for P1 is shown in Figure S11.

**Poly[3-(6-methylsulfonylhexyl)thiophene] (P2).** P-MeST (0.15 g) was dissolved in 20 mL of dichloromethane in a 50 mL one-neck round-bottom flask and stirred at 25 °C. Purified *m*-CPBA (0.27 g, 1.5 mmol) was dissolved in 2 mL of dichloromethane, and the solution was added dropwise into the flask in 10 min. After stirring at 25 °C for 5 min, the reaction was poured into diethyl ether to precipitate the product. The precipitate was collected into a Soxhlet thimble and extracted with diethyl ether and chloroform. The product was collected from the chloroform fraction. After evaporating chloroform, P2 was obtained as a dark green solid (80 mg, 46% isolated yield).  $^1H$  NMR (500 MHz,  $CDCl_3$ ,  $\delta$ ): 6.96 (s, =CH-, 1H), 2.95–3.04 (m,  $-SO_2CH_2-$ , 2H), 2.87 (s,  $-SO_2CH_3$ , 3H), 2.70–2.83 (m,  $-ArCH_2-$ , 2H), 1.79–1.92 (m,  $-SO_2CH_2CH_2-$ , 2H), 1.64–1.77 (m,  $-ArCH_2CH_2-$ , 2H), 1.38–1.58 (m,  $-SO_2CH_2CH_2CH_2CH_2-$ , 4H) (Figure S8). Elemental analysis: Calcd for  $(C_{11}H_{16}O_2S_2)_n$ : C 53.46%; H 6.55%; S 25.95%. Found: C 53.24%; H 6.21%; S 24.54%. MALDI-TOF MS for P2 is shown in Figure S12.

**Poly[3-(6-(3-methylsulfonylpropylcarbonyloxy)hexyl)thiophene] (P3).** P-BrHT (0.15 g) and 1 (0.4 g, 2 mmol) were added into a 50 mL one-neck round-bottom flask which was vacuumed and purged with  $N_2$  three times. Dry THF (8 mL) and anhydrous DMF (18 mL) were added to the flask using syringes and stirred at 50 °C under  $N_2$  for 72 h. The reaction was cooled to room temperature and poured into methanol to precipitate the product. The precipitate was collected into a Soxhlet thimble and extracted with methanol and chloroform. The product was collected into the chloroform fraction. After evaporating chloroform, P3 was obtained as a brown solid film (0.18 g, 89% isolated yield).  $^1H$  NMR (500 MHz,  $CDCl_3$ ,  $\delta$ ): 6.96 (s, =CH-, 1H) 4.07 (t,  $J = 6.5$  Hz,  $-COOCH_2-$ , 2H), 3.03–3.13 (m,  $-SO_2CH_2-$ , 2H), 2.87 (s,  $-SO_2CH_3$ , 3H), 2.71–2.84 (m,  $-ArCH_2-$ ,

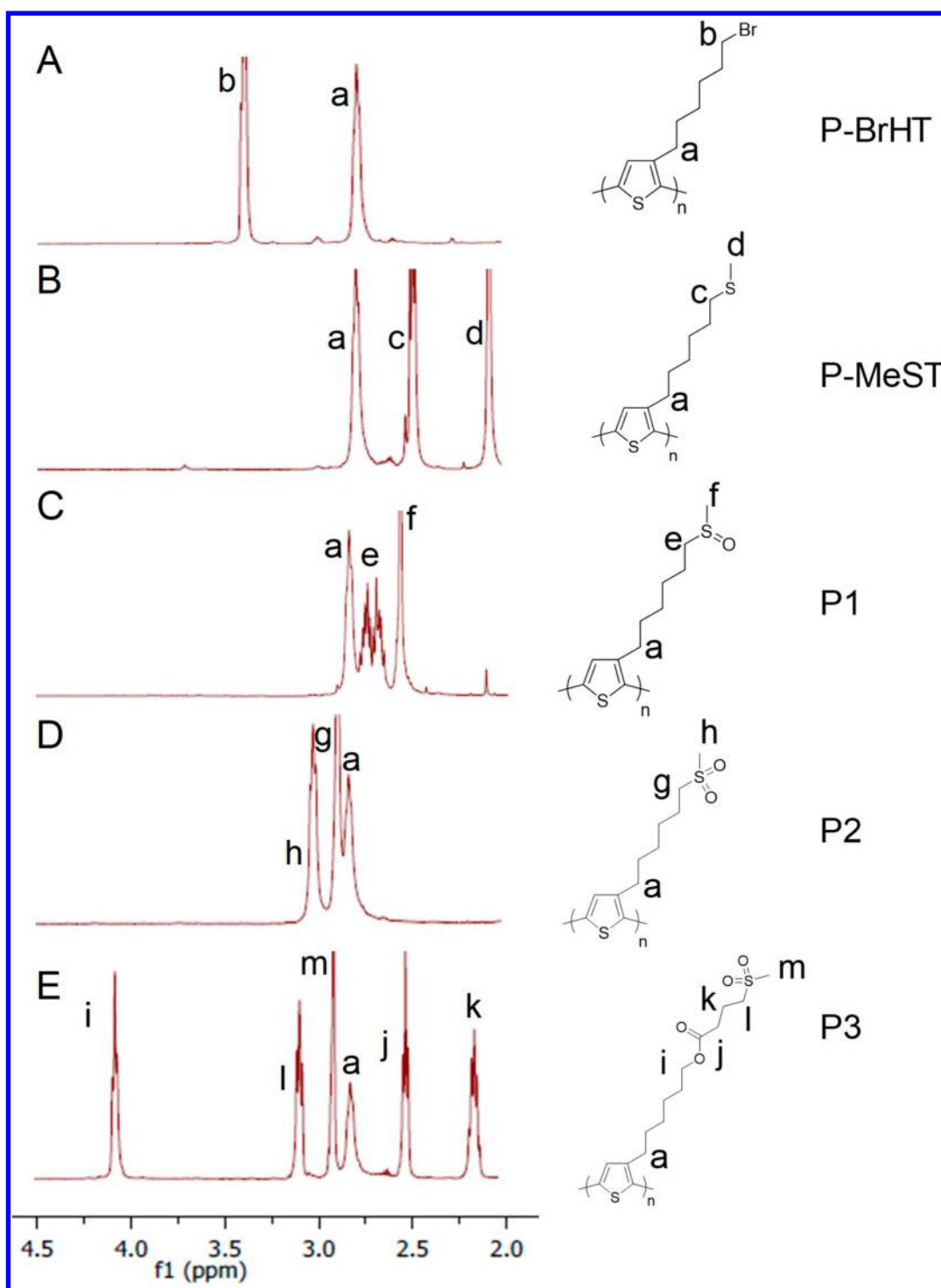


**Figure 1.**  $^1\text{H}$  NMR of spectra of various functionalized P3AT polymers in  $\text{CDCl}_3$ : (A) P-BrHT, (B) P-MeST, (C) P1, (D) P2, and (E) P3.

2H), 2.49 (t,  $-\text{OOCCH}_2-$ ,  $J = 6.9$  Hz, 2H), 2.07–2.17 (m,  $-\text{SO}_2\text{CH}_2\text{CH}_2-$ , 2H), 1.56–1.65 (m,  $-\text{ArCH}_2\text{CH}_2-$ , 2H), 1.65–1.75 (m,  $-\text{COOCH}_2\text{CH}_2-$ , 2H), 1.34–1.50 (m,  $-\text{COOCH}_2\text{C}-\text{H}_2\text{CH}_2\text{CH}_2-$ , 4H) (Figure S9). Elemental analysis: Calcd for  $(\text{C}_{15}\text{H}_{22}\text{O}_4\text{S}_2)_n$ : C 54.51%; H 6.74%; S 19.41%. Found: C 54.72%, H 6.51%, S 19.69%. MALDI-TOF MS for P3 is shown in Figure S13.

## RESULTS AND DISCUSSION

**Monomer and Polymer Syntheses.** Synthesis routes for functionalized P3AT polymers are shown in Scheme 1. The precursor poly[3-(6-bromohexyl)thiophene] (P-BrHT) was

synthesized using the published method by McCullough.<sup>29</sup> The structure of P-BrHT was confirmed by MALDI-TOF (Figure S10). The measured repeat unit mass for P-BrHT (245.03  $m/z$ ) is close to the calculated mass of repeat unit (245.01  $m/z$ ). The average molar molecular weight of P-BrHT was estimated by SEC at 10800 g/mol, about 44 repeat units. The bromines in P-BrHT were substituted with methyl thioether groups by reacting with sodium thiomethoxide in DMF (P-MeST in Scheme 1a).<sup>33</sup> The  $^1\text{H}$  NMR spectra of P-BrHT and P-MeST are shown in Figures 1A and 1B, respectively. Peak b at 3.5 ppm was assigned to the  $\text{CH}_2$

next to the bromine at the chain end of P-BrHT. In P-MeST, the methylene protons next to the bromine (peak b) completely disappeared, indicating that the  $S_N2$  reaction was quantitative. About 1.1 equiv of *m*-CPBA was used to react with P-MeST at 0 °C for 40 min to obtain P1. The  $^1H$  NMR spectrum in Figure S7 indicates that the oxidizations from P-MeST to P1 was selective and quantitative, with no obvious oxidization of the sulfinyl group and thiophenic sulfur was observed. The successful oxidization of the  $-SCH_3$  groups in P-MeST was also confirmed by FTIR, as shown in Figure 2. In

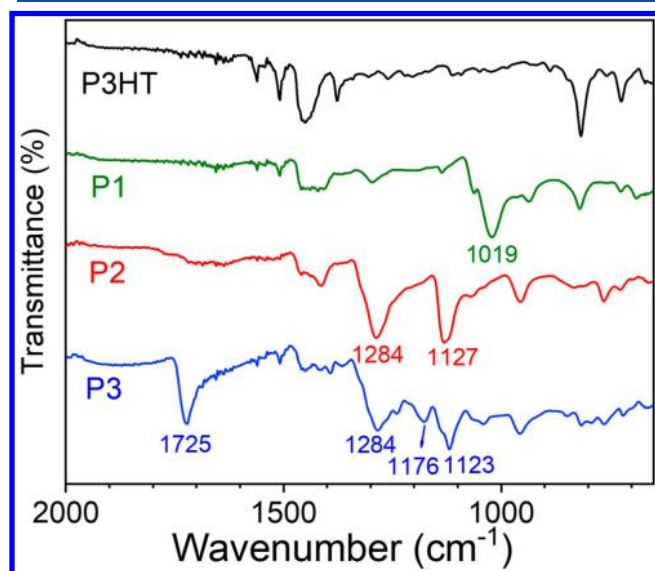


Figure 2. Transmission FTIR spectra of P3HT, P1, P2, and P3.

P1, the peak at  $1019\text{ cm}^{-1}$  was attributed to the  $S=O$  stretching in the sulfinyl group. MALDI-TOF in Figure S11 also confirms the repeat-unit mass of P1 (observed  $229.42\text{ m/z}$  and calculated  $230.08\text{ m/z}$ ).

P2 was synthesized by using 2.5 equiv of *m*-CPBA as oxidizer under 25 °C, and  $^1H$  NMR indicated that all  $-SCH_3$  groups in P-MeST were oxidized into methylsulfonyl groups (Figure S8A). The successful oxidization was further confirmed by FTIR, as shown in Figure 2. The peak at  $1019\text{ cm}^{-1}$  disappeared and peaks at  $1284$  and  $1127\text{ cm}^{-1}$  appeared, due to the asymmetric and symmetric  $O=S=O$  stretching, respectively. MALDI-TOF in Figure S12 also confirms the repeat-unit mass of P2 (observed  $246.01\text{ m/z}$  and calculated  $246.07\text{ m/z}$ ). Because of solubility issues, we could not measure  $M_n$  for P1 and P2 by SEC.

Nucleophile **1** was obtained by a three-step reaction, as shown in Scheme 1b, with an overall yield of 17%. Nucleophile **1** was then reacted with P-BrHT to obtain P3 with side chains containing one sulfonyl and one ester groups, separated by three  $CH_2$  groups (see Scheme 1C). The  $^1H$  NMR spectrum of P3 (Figure 1E) shows that peak b completely disappeared, indicating a quantitative  $S_N2$  reaction. FTIR confirmed the presence of ester and sulfonyl groups in P3: the absorption bands at  $1725$  and  $1176\text{ cm}^{-1}$  corresponded to the  $C=O$  and  $C-O$  stretching in the ester group, respectively, and the absorption bands at  $1284$  and  $1123\text{ cm}^{-1}$  corresponded to the asymmetric and symmetric  $O=S=O$  stretching, respectively. MALDI-TOF in Figure S13 also confirms the repeat-unit mass of P3 (observed  $330.50\text{ m/z}$  and calculated  $331.11\text{ m/z}$ ).

The solubility of these functionalized P3AT polymers was strongly affected by the polar groups at the side-chain ends: P1, P2, and P3 were more soluble in polar solvents and less soluble in nonpolar solvents, as compared to P3HT. P3HT was readily soluble in chlorinated solvents such as chloroform and dichlorobenzene, and insoluble in polar solvents such as DMF and dimethyl sulfoxide (DMSO). On the other hand, P1, P2, and P3 were insoluble in dichlorobenzene, but soluble in DMF and DMSO ( $<25\text{ mg/mL}$ ). P1 and P3 had a high solubility, i.e.,  $>30\text{ mg/mL}$ , in chloroform, whereas P2 had a low solubility of  $<5\text{ mg/mL}$  in chloroform. We found that P1, P2, and P3 all had good solubilities of  $>30\text{ mg/mL}$  in chloroform with 6 vol % of methanol (see light scattering results in Figure S14). Sulfonyl groups are polar and tend to aggregate in nonpolar solvents, such as chloroform or dichlorobenzene. The addition of some polar solvents, such as methanol or ethanol, could break the aggregation and increase the solubility of P1–P3 in a low-polarity solvent.

**Thermal Properties.** TGA results are shown in Figure 3. For P3HT, only one thermal degradation process was observed

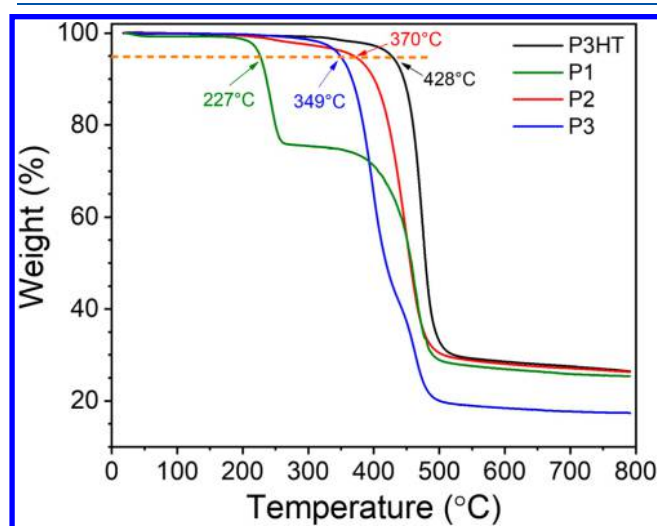
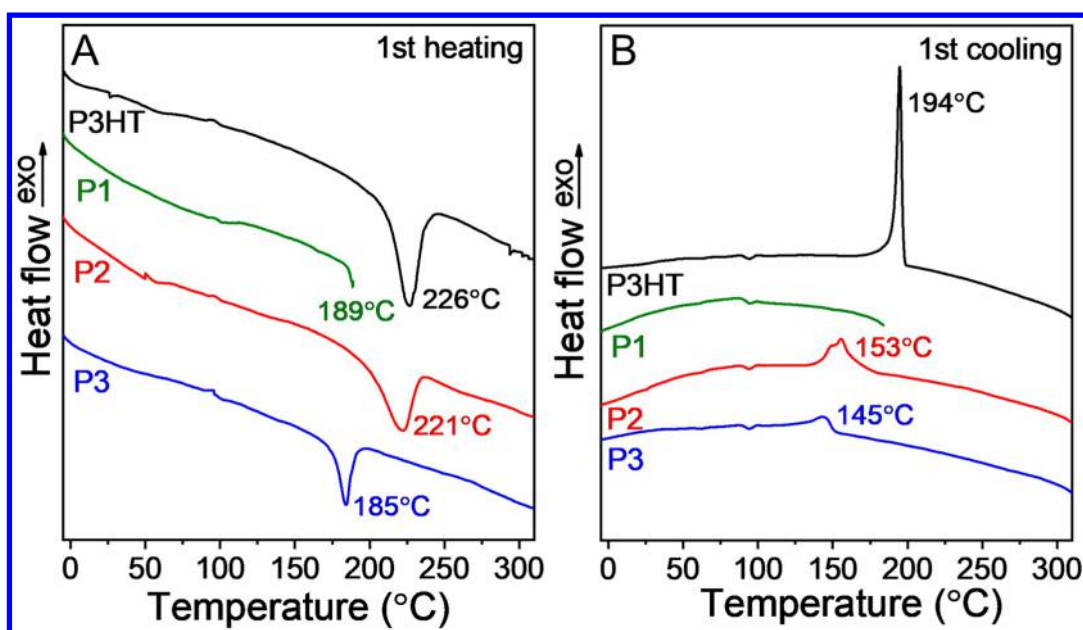


Figure 3. TGA curves for P3HT, P1, P2, and P3. The heating rate was  $20\text{ °C/min}$  under a dry nitrogen flow.

with a 5% weight loss at  $428\text{ °C}$ , which is close to the reported value of  $440\text{ °C}$ .<sup>34</sup> P1 showed a 24% weight loss from 227 to  $250\text{ °C}$ , corresponding to the weight loss of the methylsulfonyl group. P3 showed  $\sim 50\%$  weight loss from 349 to  $417\text{ °C}$  due to the loss of methylsulfonyl and ester groups. While side chain functionalization decreased the polymer stability relative to neat P3HT, all polymers were stable below  $200\text{ °C}$ , which should be sufficient for most device fabrication conditions.

These functionalized P3AT polymers were crystalline, and their melting and crystallization behavior were studied by DSC (Figure 4). All solution-cast samples were heated from  $-10$  to  $320\text{ °C}$  at a ramp rate of  $10\text{ °C/min}$ , except for P1, which was heated from  $-10$  to  $190\text{ °C}$  to avoid thermal degradation. For P3HT, the observed melting temperature ( $T_m$ ) at  $226\text{ °C}$  and the crystallization temperature ( $T_c$ ) at  $194\text{ °C}$  were close to reported values.<sup>34</sup> P1 started to melt around  $189\text{ °C}$  at the end of the first heating cycle, before significant thermal degradation happened. Both P2 and P3 had lower  $T_m$  and  $T_c$  than P3HT. The heats of fusion for all polymers during the first heating process were calculated except for P1, which did not exhibit a full melting peak in the DSC curve. P3HT had a heat of fusion



**Figure 4.** DSC curves for P3HT, P1, P2, and P3 during (A) the first heating and (B) the first cooling processes. The heating and cooling rates were 10 °C/min. DSC samples were prepared by drop-casting polymers from chloroform with 6 vol % methanol in DSC pans.

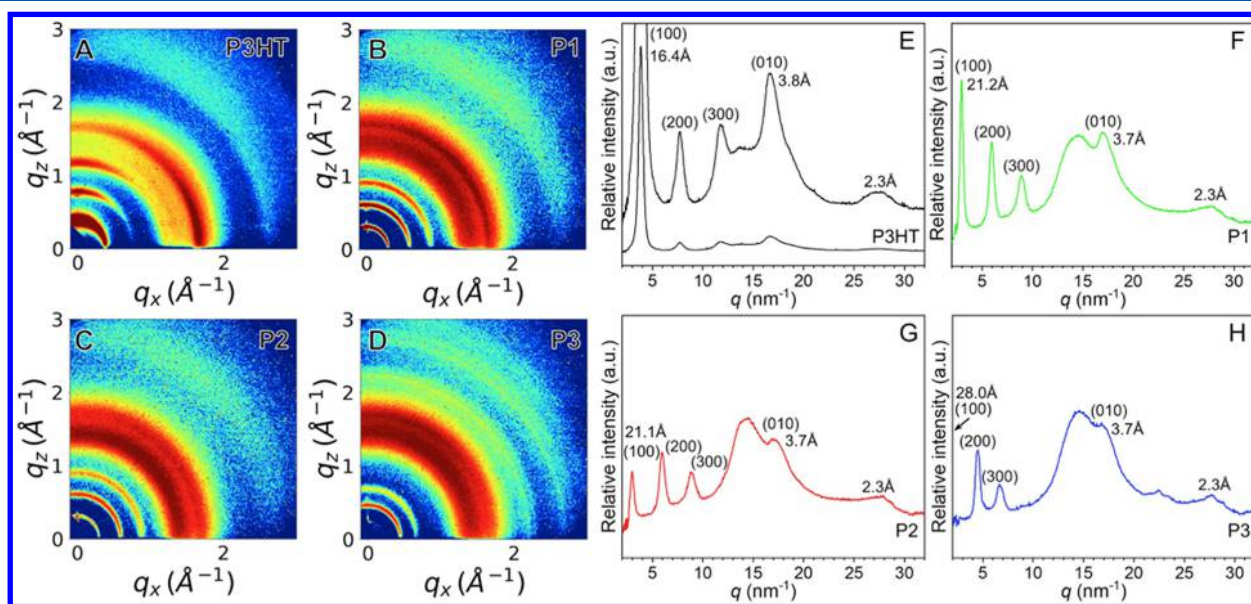


**Figure 5.** 2D GI-WAXD patterns of (A) P3HT, (B) P1, (C) P2, and (D) P3 measured for solution-cast thin films ( $\sim 1 \mu\text{m}$  thick) and (b) 1D WAXD profiles of (E) P3HT, (F) P1, (G) P2, and (H) P3 integrated from the corresponding GI-WAXD patterns in (A–D).

( $\Delta H_f$ ) of 20.0 J/g, and the crystallinity was calculated to be 41% by using the heat of fusion ( $\Delta H_f^0$ ) of 49 J/g for 100% crystalline P3HT.<sup>35</sup> The heats of fusion for P2 (11.0 J/g) and P3 (6.5 J/g) were significantly lower than that of P3HT. Their crystallinities are not calculated because no  $\Delta H_f^0$  values are available for P1–P3. Glass transitions for P1–P3 could not be clearly identified from DSC. We speculate that this results from a combination of rigid conjugated backbone with highly interacting dipoles in the side chains of P1–P3, resulting in a small entropy change before and after the glass transition.

**GI-WAXD.** The effects of the sulfinyl and sulfonyl functional groups on the crystalline structure and  $\pi$ - $\pi$  stacking in solution-cast films were investigated by GI-WAXD. As shown in Figure 5A, the GI-WAXD pattern of P3HT exhibited well-oriented (100) reflection in the vertical direction and (010)

reflection (i.e., the  $\pi$ - $\pi$  stacking) in the horizontal direction, indicating the monoclinic crystalline structure with horizontal lamellar stacking and edge-on P3HT orientation.<sup>36</sup> From the integrated 1D profile in Figure 5E, the crystallinity for P3HT was estimated to be 80%; however, this estimation is inaccurate because the solution-cast P3HT film exhibited an obvious crystal orientation in Figure 5A. For P1–P3 films, no crystal orientation was observed in the 2D GI-WAXD patterns (Figure 5B–D); therefore, the crystallinity estimation from the 1D GI-WAXD profiles should be more accurate. It is possible that the crystallite sizes were so small that a random crystal orientation existed in solution-cast P1–P3 films. From the 1D profiles (Figure 5F–H), crystallinities were estimated to be 36% for P1, 31% for P2, and 32.5% for P3. Note that the  $\pi$ - $\pi$

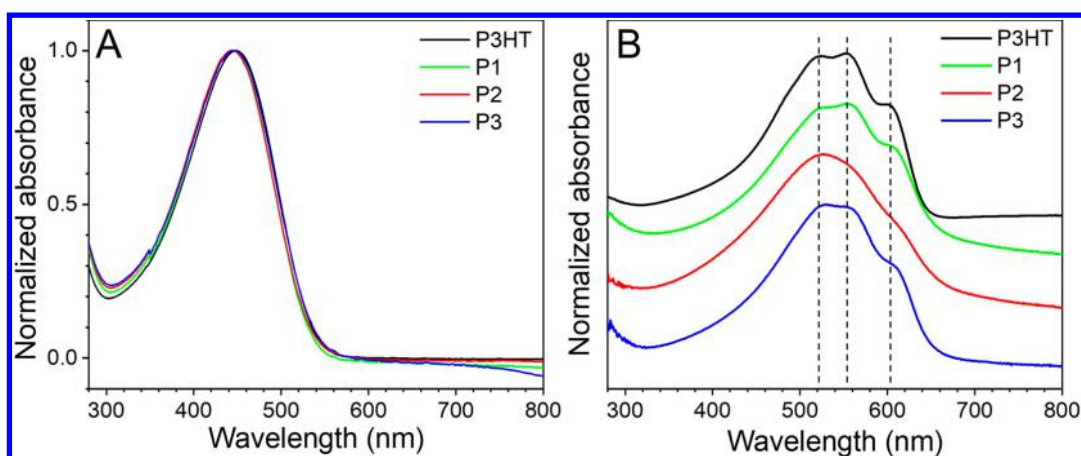


**Figure 6.** UV-vis absorption spectra of P3HT, P1, P2, and P3 in (A) solution and (B) spin-coated thin films (around 65 nm). All absorbance intensities are normalized. In (B), curves are offset for clarity.

**Table 1. Physical and Optical Properties of P3HT and Functionalized P1–P3<sup>a</sup>**

polymer	$M_n$ (kDa)	PDI	solution		film		$E_{g,opt}$ (eV)	HOMO (eV)	LUMO (eV)
			$\lambda_{max}$ (nm)	$\lambda_{onset}$ (nm)	$\lambda_{max}$ (nm)	$\lambda_{onset}$ (nm)			
P3HT	9.9	1.3	450	534	525, 552, 601	643	1.93	-5.15	-3.22
P1	11.3	1.28	445	531	530, 554, 602	674	1.84	-5.24	-3.40
P2	12.1	1.28	444	531	528	658	1.88	-5.22	-3.34
P3	16.3	1.28	446	535	530, 554, 604	686	1.81	-5.21	-3.40

<sup>a</sup>Polymer films (around 65 nm) were spin-coated from chloroform with 6 vol % methanol. HOMO energy levels were estimated from the onset of the oxidation waves using the value of -5.1 eV for Fc/Fc<sup>+</sup>. Optical band gap ( $E_{g,opt}$ ) values were estimated from the thin film UV-vis absorbance. Lowest unoccupied molecular orbital (LUMO) values were calculated by adding values of  $E_{g,opt}$  to the HOMO levels.  $M_n$ s of P1, P2, and P3 were calculated by assuming the degrees of polymerization (DPs) of P1, P2, and P3 were the same as that of the precursor P-BrHT (DP ~ 44).

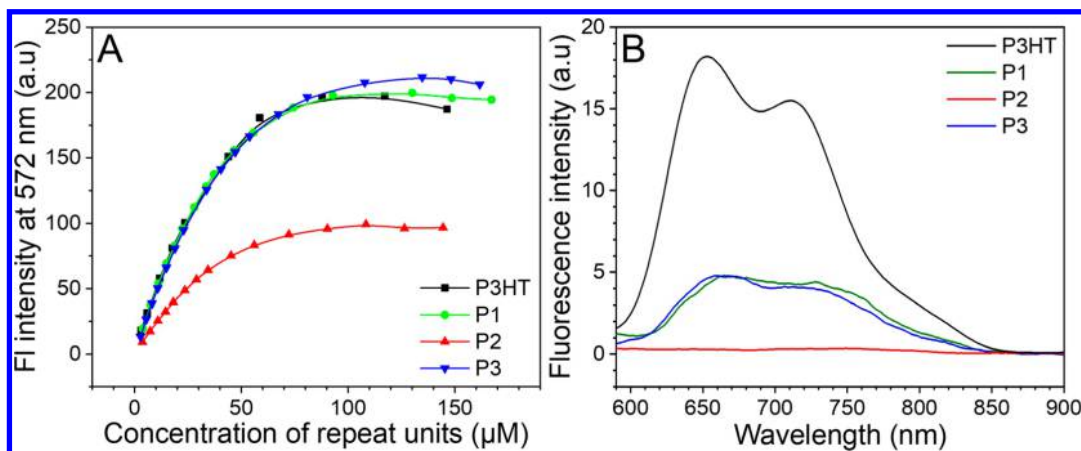


**Figure 7.** (A) Fluorescence intensity at 572 nm as a function of the repeat-unit concentration in solution (i.e., chloroform with 6 vol % methanol) and (B) fluorescence spectra in spin-coated thin films (~65 nm thick) for P3HT, P1, P2, and P3.

stacking in P1–P3 became much poorer compared to P3HT, as reflected by weak (010) reflections around  $17.0 \text{ nm}^{-1}$ .

**Optical Properties.** UV-vis absorption spectra of functionalized P3ATs were measured in both solution (Figure 6A) and spin-coated films (Figure 6B). Results are summarized in Table 1. All polymers had similar absorption spectra in solution, indicating that the functional groups did not electronically couple with the polythiophene backbone. Upon film formation, all absorption spectra red-shifted, indicating that the polythiophene backbones planarized upon film formation. The spectrum of the P3HT film showed three obvious vibronic peaks at 522, 555, and 600 nm, which were attributed to the intermolecular  $\pi$ - $\pi$  interactions in the

crystalline phase.<sup>37,38</sup> P1 had similar vibronic peaks as P3HT, indicating that the addition of sulfinyl groups at the end of P3AT side chains did not significantly destroy the long-range  $\pi$ - $\pi$  interactions. Similarly, P3 also had three vibronic peaks, though weaker than those of P3HT. On the contrary, P2 did not show obvious vibronic peaks, and possible reasons will be discussed later.

Figure 7A depicts the fluorescence intensity at 572 nm as a function of the repeat-unit concentration of functionalized P3AT polymers in solution. Although all polymers exhibited the same normalized fluorescence spectra in solution (see Figure S15), the fluorescence intensity at 572 nm appeared to be different for different polymers. From Figure 7A,

fluorescence intensities of all polymers had a linear relationship with the repeat-unit concentration when the concentration was below  $\sim 20 \mu\text{M}$ . Upon further increasing the repeat-unit concentration, fluorescence intensities started to level off and reached a plateau value. The plateau fluorescence intensities of P3HT, P1, and P3 were similar, i.e., around 195 au. However, P2 exhibited a much lower plateau fluorescence intensity, only 95 au, nearly half of those for P3HT, P1, and P3. Film fluorescence of these polymers was measured to investigate how functional groups affect the emission in the solid state (Figure 7B). Even though all spin-coated films had a similar thickness ( $\sim 65 \text{ nm}$ ) and were measured under the same conditions, large differences in the fluorescence intensity were observed depending on the polar groups in side chains. P3HT had the strongest fluorescence intensity, followed by P1 and P3 with similar but much lower fluorescence intensities and P2 with negligible fluorescence emission. Obviously, the fluorescence-quenching effect was amplified for P1–P3 in films with P2 almost completely quenched. For P1 and P3, sulfinyl and sulfonyl groups in the side chains may be interacting with the polythiophene backbone, facilitating vibrational relaxation and thus attenuating the fluorescence emission. For P2, there must be an additional reason for the complete fluorescence quenching.

Considering the large difference in polarity between polar sulfonyl side chains and hydrophobic polythiophene backbones, it is likely that micelles could form for P1–P3 in the chloroform with 6 vol % methanol. Consequently, this might affect the optical properties of functionalized P3AT polymers.<sup>39,40</sup> To test this speculation, AFM was used to study the surface morphologies of solution-cast films for P3HT and P1–P3 (see Figure S16). The surfaces of P3HT and P1 were relatively smooth without any signs of micelle formation, whereas P2 and P3 films showed typical micellar morphology with average micelle sizes around 50–100 nm. Giving the fact that P1 and P3 films showed similar fluorescence intensity (Figure 7B) while P3 formed micelles and P1 did not form micelles in films, micelle formation could not explain fluorescence quenching observed for the solid film.

Wei et al. found that oxidized thiophene units in the polythiophene main chain could drastically decrease the fluorescence in solutions.<sup>41</sup> Because the fluorescence of P2 was significantly lower in both solution and film compared to other polymers, we surmise that P2 might contain intrinsic defects in the polymer backbone, such as oxidized thiophenic units. Note that *m*-CPBA was used to oxidize thiophene at room temperature.<sup>42</sup> Although it took a long time for the thiophene oxidation to happen, it was still possible that a small amount of thiophenic units in P-MeST was oxidized by *m*-CPBA during the reaction. Careful inspection of the  $^1\text{H}$  NMR spectrum of P2 in Figure S8A confirmed a small amount of oxidized thiophenic units: the integral of proton on the thiophenic unit (peak a, 0.91) was lower than the expected value of 1.0, and a small peak around 7.5 ppm was seen. To help assign this peak, an overoxidized P2 was purposely synthesized by reacting 4 equiv of *m*-CPBA with P-MeST, and the  $^1\text{H}$  NMR spectrum of the overoxidized P2 is shown in Figure S8B. The proton signal around 7.5 ppm was larger and is assigned to the proton on the oxidized thiophenic units.<sup>43</sup> In addition, the proton signal (peak a') from oxidized thiophenic units and the peak for  $\text{CH}_2$  protons adjacent to the oxidized thiophenic unit (i.e., peak b in Figure S8B) were also observed. To study the effect of the intrinsic defects in P2 on

fluorescence quenching, we blended P3HT with P2 at different ratios. As shown in Figure S17A,B, the fluorescence emission gradually quenched and the vibronic peaks gradually disappeared upon addition of P2 into P3HT in thin films. In this case, it is likely that P2 and P3HT formed miscible blends in the solid state and that the oxidized defects in P2 caused weakening of vibronic peaks and quenching of fluorescence.

**Electrochemical Properties.** Figure 8 depicts the cyclic voltammograms (CV) of P3HT and the functionalized P3AT

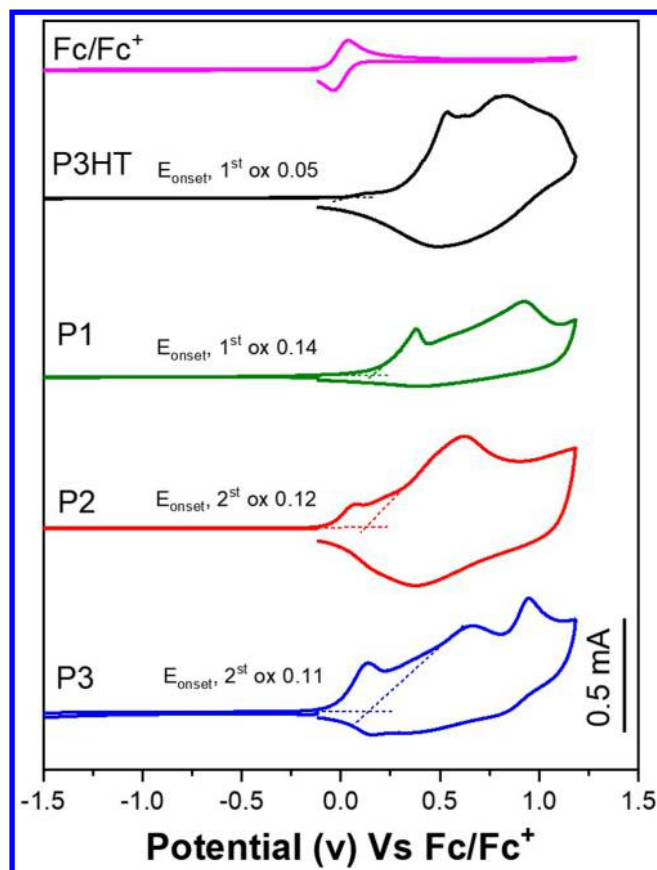


**Figure 8.** Thin film cyclic voltammetry (CV) curves for P3HT, P1, P2, and P3. Fc/Fc<sup>+</sup> was used as internal standard.

polymers in thin films. The oxidation onset potentials were used to estimate the HOMO energy levels. For P3HT, the small peak around 0.1 V was considered as the first oxidation peak, and the first onset oxidation potential versus Fc/Fc<sup>+</sup> was calculated to be 0.05 V. From this onset, the HOMO energy level of P3HT was estimated to be  $-5.15 \text{ eV}$ .<sup>44</sup> For P1, the first onset oxidation potential versus Fc/Fc<sup>+</sup> was 0.14 V, and the HOMO energy level was estimated to be  $-5.24 \text{ eV}$ . For P2 and P3, there existed a first oxidation peak  $\sim 0.1 \text{ V}$ , which was more positive than expected for oxidation of the polythiophene backbone. To elucidate the nature of this oxidation, we measured the CV spectra of P2, P3, and R-P3, a small molecule that contained sulfonyl groups in DMF, as shown in Figure S18. Ethyl acetate (which contains an ester group) and dimethyl sulfoxide (which contains a sulfinyl group) both did not show any peaks in the measurable spectrochemical window. On the other hand, molecule R-P3 (which contains a sulfonyl group) had an oxidation peak  $\sim 0.26 \text{ V}$ , very similar to the first oxidation peaks observed for P2 and P3 in solution. Therefore, we attribute the first oxidation peak to oxidation of

the sulfonyl groups in P2 and P3. To estimate the HOMO energy levels of P2 and P3, we therefore used the second onset of the oxidation potentials versus Fc/Fc<sup>+</sup>, and they were 0.12 V for P2 and 0.11 V for P3. The corresponding HOMO energy levels were estimated to be -5.22 and -5.21 eV for P2 and P3, respectively. The lowest unoccupied molecular orbital (LUMO) energy levels were estimated using the optical band gap ( $E_{g,opt}$ ) values and are reported in Table 1.

**Dielectric Properties.** It is difficult to accurately measure the dielectric constant of semiconducting polymers because conduction of space charges (i.e., electrons and holes and sometimes impurity ions) can significantly prevent the accurate measurement of the capacitance from electronic, atomic, and dipolar polarizations.<sup>15,16</sup> First, directly sandwiching the semiconductor between two metal electrodes [or with a poly(3,4-ethylenedioxythiophene)-polystyrenesulfonate (PEDOT-PSS) hole-conducting/electron-limiting layer] should not be used to measure dielectric constants by BDS or impedance spectroscopy because the high conductance of mobile space charges shorts the sample, especially at low frequencies. To prevent the direct shorting of the sample from space charge conduction, at least a bilayer structure composed of a semiconducting polymer and a highly insulating dielectric layer such as SiO<sub>2</sub> should be used, as reported in the literature.<sup>23</sup>

In this study, we tested this method for P3HT and P1-P3. A gold/semiconducting polymer/SiO<sub>2</sub>/n-doped Si device was used following the literature report.<sup>23</sup> The n-Si substrate and the gold coating served as conductive electrodes. The SiO<sub>2</sub> layer was made by wet-etching chemistry, rather than the dry O<sub>2</sub> oxidation method. It had a thickness of 230 ± 10 nm and was used as the insulating dielectric layer to block the leakage current from space charges in the semiconducting polymer. Compared to the thin SiO<sub>2</sub> layer, a thick (5–10 μm) polymer film was drop-cast on the top of the SiO<sub>2</sub> layer. In such a way, the capacitance of the semiconducting polymer layer ( $C_p$ ) was smaller than that of the SiO<sub>2</sub> layer ( $C_{Si}$ ). Without any conduction of space charges, the measured bilayer capacitance ( $C$ ) is  $1/C = 1/C_p + 1/C_{Si}$ . Because  $C_p$  is smaller than  $C_{Si}$ , the bilayer  $C$  is close to  $C_p$ , and the system errors from surface roughness and pinholes in the semiconducting polymer layer can be minimized.

The bottom n-Si wafer was a continuous electrode (ca. 1 in.<sup>2</sup>). The top gold electrode had a discrete circular shape with a diameter of 2.4 mm. In such a configuration, there was a problem of conduction when the semiconducting polymer layer was a continuous film. Because the SiO<sub>2</sub> layer was prepared from wet-etching chemistry, there were some pinholes with an estimated density of 1 per 10–20 mm<sup>2</sup>. With a continuous semiconducting polymer layer, the top gold electrode could short-circuit with the bottom n-Si electrode through the continuous polymer layer. To avoid this problem, the polymer was isolated by carefully wiping off the polymer around the top gold electrode using a cotton swab soaked with acetone. By doing so, we were able to obtain about 5–6 successful devices out of 10 samples for the dielectric constant measurement.

One way to eliminate the effect of space charge conduction is to apply a dc bias voltage to the bilayer capacitor to deplete space charges in the semiconducting polymer layer (i.e., by recombination of electrons from the negative gold electrode and holes in the p-type polymer), while measuring the bilayer capacitance using a sinusoidal driving voltage (the root-mean-

square voltage,  $V_{rms} = 1$  V), as described in a previous report.<sup>23</sup> Then,  $C_p$  and thus dielectric constant of the semiconducting polymer can be extracted from the bilayer capacitance, when space charges are depleted. To test the suitability of this idea, the capacitance of the P3HT/SiO<sub>2</sub> bilayer capacitor was measured by sweeping the bias voltage from -50 to +150 V at room temperature with different frequencies of the measuring ac voltage (1 V<sub>rms</sub>), as shown in Figure S19. When the bias voltage was negative, the capacitance remained constant (ca.  $6.1 \times 10^{-10}$  F), which was the capacitance of the SiO<sub>2</sub> layer [ $C_{Si} = \epsilon_{r,Si}\epsilon_0 A/d = 6.15 \times 10^{-10}$  F, where  $\epsilon_{r,Si}$  is the relative permittivity of SiO<sub>2</sub> (4.0, and also see our BDS data in Figure S20,  $\epsilon_0$  is the vacuum permittivity,  $A$  is the sample area (4.52 mm<sup>2</sup>), and  $d$  is the thickness of the SiO<sub>2</sub> layer]. When the bias voltage changed to positive values (see Figure S19A), the bilayer capacitance started to drop, indicating that holes in the P3HT layer were gradually depleted by the electrons from the negative gold electrode. However, the bilayer capacitance did not reach a saturation even when the bias voltage was 100 V (see Figure S19B). Using the capacitance value at 100 V bias voltage, we calculated the dielectric constant for P3HT to be 2.9, which is lower than the literature value of 3.8.<sup>45</sup> This measurement method was also applied to functionalized P3HT samples (i.e., P1-P3); however, complete depletion of holes could not be reached even when the bias voltage was as high as 200 V (data not shown). This result indicated that this method could not be generalized for different semiconducting polymers. In addition, a high bias voltage should be avoided for dielectric measurements because of the high risk for dielectric breakdown. For example, breakdown was observed at 10 Hz when the bias voltage increased to 50 V and above in Figure S19B.

Rather than using a high dc bias voltage, a high frequency could be used to stop the conduction of space charges because it is known that above a certain frequency, migration of impurity ions in a polar polymer vanishes.<sup>46</sup> In other words, low-voltage BDS could be directly used to measure the dielectric constant of semiconducting polymers for the bilayer sample geometry in Figure S19A. Figure S21A,B shows frequency-scan BDS results for the real ( $C'$ ) and imaginary ( $C''$ ) parts of the measured complex capacitance ( $C^*$ ) of the bilayer P3HT/SiO<sub>2</sub> sample. When the pristine sample was measured in air, the  $C'$  reached a maximum value of  $6.1 \times 10^{-10}$  F below 10<sup>2</sup> Hz and a minimum value of  $2 \times 10^{-11}$  F above 10<sup>5</sup> Hz. Again, the low-frequency  $C'$  value was the same as that of the SiO<sub>2</sub> layer, indicating that P3HT became conductive at low frequencies due to the high mobility of holes. Above 10<sup>5</sup> Hz, holes could not catch up with the fast switching ac voltage, leading to series capacitors of SiO<sub>2</sub> and P3HT. Between these two frequencies, holes started to migrate and P3HT gradually lost the capability of storing electric energy. From the bilayer capacitance, the dielectric constant of P3HT at room temperature was calculated to be 3.75, which is consistent with the reported value.<sup>45</sup> However, the window for series SiO<sub>2</sub> and P3HT capacitors was rather narrow, only from 10<sup>5</sup> to 10<sup>6</sup> Hz. To broaden this frequency window, thermal annealing at 100 °C for 1 h was performed in a dry N<sub>2</sub> atmosphere (i.e., in the Novocontrol sample chamber). After annealing, the frequency window extended down to 10 Hz. Meanwhile, there was a peak observed in the  $C''$  plot in Figure S21B, which could be attributed to the conduction of holes in P3HT.<sup>47</sup> This conduction peak shifted from 300 Hz for the sample in air to 0.3 Hz for the thermally annealed sample in

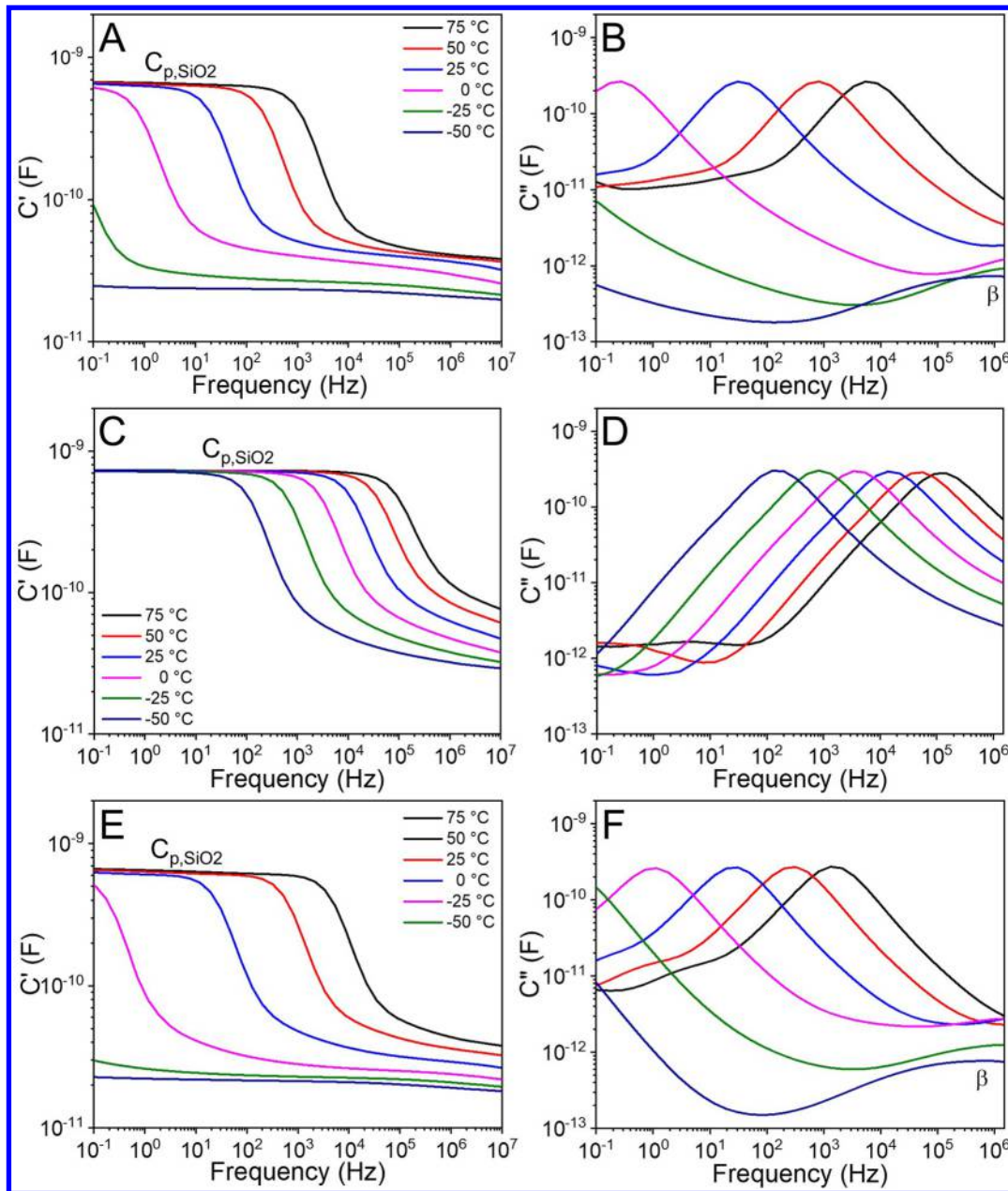


**Figure 9.** Frequency-scan (A, C, E) real ( $C'$ ), and (B, D, F) imaginary ( $C''$ ) parts of the bilayer capacitance at various temperatures for (A, B) P1, (C, D) P2, and (E, F) P3. The layer thicknesses for P1, P2, and P3 are 9.3, 9.3, and 8.1  $\mu\text{m}$ , respectively. The standard deviation of film thicknesses was around 10%.

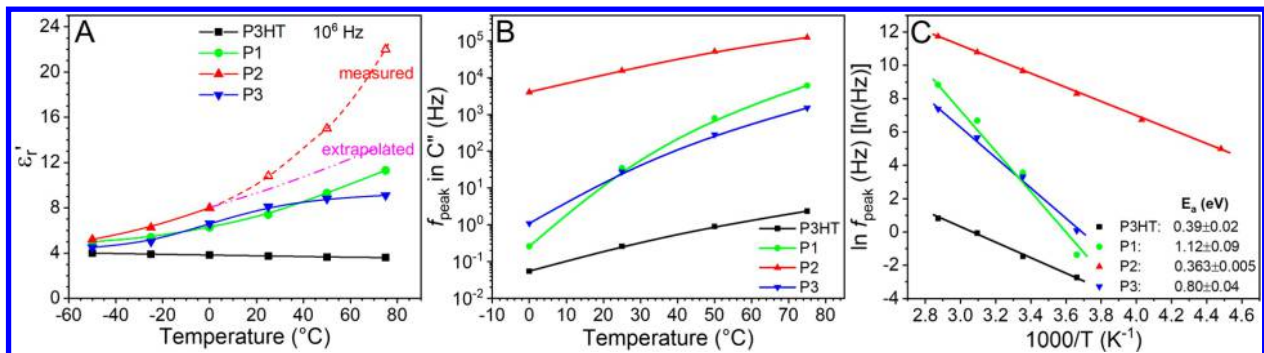


**Figure 10.** (A) Dielectric constants as a function of temperature for P3HT, P1, P2, and P3, calculated from the  $C'$  values at  $10^6$  Hz in Figures S19C and 9A,C,E. (B) Plot of  $\ln f_{\text{peak}}$  as a function of  $1/T$  for P3HT, P1, P2, and P3. The activation energy ( $E_a$ ) values are calculated from the slopes in (C).

$N_2$ . Similar peaks were also observed for the conduction of impurity ions in polar polymers such as poly(vinylidene fluoride) (PVDF), and the peak position was related to the mobility of impurity ions.<sup>48,49</sup> Therefore, the shift of the  $C''$  peak to a lower frequency after thermal annealing in  $N_2$  might suggest that the hole mobility decreased after removing  $O_2$  from the sample. Namely, P3HT was dedoped. While  $O_2$  doping of P3HT is known to increase conductivity via introducing more holes into the polymer,<sup>50</sup> it has also been shown to improve mobility.<sup>51</sup> A similar doping effect on charge carrier mobility was also reported for high dielectric constant 2D molybdenum oxide.<sup>52</sup> For the rest of this dielectric study, all samples (P3HT and P1–P3) were thermally annealed at 100 °C for 1 h to minimize  $O_2$  doping. By lowering the temperature, the hole mobility further decreased and the hole conduction peak continuously shifted to lower frequencies, as shown in Figure S19C,D. Nonetheless, the dielectric constant of P3HT changed only slightly between 3.6 and 4.0.

Frequency-scan BDS was applied to P1, P2, and P3 at different temperatures, and results are shown in Figure 9. Similar to the case for P3HT in Figure S21, dielectric constants of P1–P3 could be calculated from the  $C'$  values at  $10^6$  Hz, as long as the  $C'$  had almost reached the plateau value (i.e., free of the influence from hole migration/conduction). Figure 10A summarizes calculated dielectric constants at different temperatures for P3HT and P1–P3. At  $-50$  °C (and below), the dielectric constants of all sample were similar, i.e., around 4–5, indicating that dipolar polarization in P1–P3 should be largely suppressed (i.e., dipoles were mostly frozen). Upon increasing the temperature, the dielectric constant for P3HT slightly decreased to 3.6 at 75 °C. On the contrary, dielectric constants for P1–P3 increased with temperature. The dielectric constants for P1 and P3 were similar, whereas that for P2 was higher. Note that at 25 °C and above the  $C'$  for P2 did not reach the minimum plateau values due to a higher conduction or possibly a higher hole mobility. Therefore, the calculated dielectric constants for P2 at 25 °C and above were not accurate, and the data are represented by the open triangle symbol in Figure 10A. To obtain a more accurate dielectric constant, an extrapolated curve was used (see the magenta curve in Figure 10A). At room temperature, the dielectric constants for P1, P2, and P3 were 7.4, 9.3, and 8.1, respectively, significantly higher than that of P3HT. The higher dielectric constant for P2 than P1 could be attributed to the larger dipole moment for the sulfonyl group (4.5 D) than that of the sulfinyl group (3.95 D). The lower dielectric constant for P3 than P2 could be attributed to the twisted conformation of side chains, where the dipole moments from ester and sulfonyl groups might cancel each other.

From Figure 10, the dielectric behaviors of P1 and P3 appeared to be similar, whereas P2 behaved differently. Basically, at the same temperature, the hole-conduction peak frequencies in  $C''$  for P1 and P3 were similar, whereas the peak in  $C''$  for P2 appeared at much higher frequencies (data are also summarized in Figure 10B). Nonetheless, all conduction peak frequencies for P1–P3 were higher than that for P3HT (see Figure S21). Because the conduction peak position in  $C''$  was not very sensitive to the polymer thickness as long as they were similar, we surmise that it should be primarily related to the hole mobility in samples. Consequently, the results in Figure 10B suggest that the hole mobilities in P1–P3 were higher than that of P3HT. Also, the hole mobilities of P1 and P3 were similar but lower than that of P2. This observation

correlated well with the order of dielectric constants for P3HT and P1–P3, as observed in Figure 10A. We consider that there should a correlation of dielectric constant with charge carrier mobility; the higher the dielectric constant, the higher the charge carrier mobility. This is consistent with the idea or proposal in our previous publication.<sup>19</sup> Increased charge carrier mobility with higher dielectric constant has also been observed for 2D molybdenum oxide.<sup>52</sup> To better quantify the charge carrier mobilities, we are currently working on theoretical simulation of the bilayer system, and results will be published in the future. Note that in Figure 8B,F, the sub- $T_g$  or  $\beta$  transition from dipole switching were observed around  $10^6$  Hz for P1 and P3, respectively. However, the  $\beta$  transition was not observed for P2 because the fast hole conduction masked it.

The temperature dependence of charge carrier mobility was studied by the  $\ln f_{\text{peak}}$  vs  $1/T$  plot in Figure 10C. A linear Arrhenius relationship was observed, and from the slopes the activation energy ( $E_a$ ) was obtained. The  $E_a$  values for P1 and P3 were around 0.8–1.12 eV, whereas those for P3HT and P2 were around 0.36–0.39 eV. These values were similar to the  $E_a$  for conduction of impurity ions in PVDF.<sup>46</sup> The higher  $E_a$  values for P1 and P3 indicated that the mobilities for P1 and P3 were more temperature dependent than those for P3HT and P2.

## ■ CONCLUSIONS

In this work, we have successfully synthesized functionalized P3AT polymers with highly dipolar methylsulfinyl or methylsulfonyl end groups in the alkyl side chains. The goal is to achieve high  $\epsilon_r$  via enhanced dipolar polarization without significantly changing the crystalline structure for the polythiophene backbones. Structural analysis based on GI-WAXD indicated that the crystalline structure of polythiophene backbones was largely preserved, although the overall crystallinity was somewhat interfered by the strong dipolar interaction among the sulfinyl and sulfonyl end groups. Using a bilayer sample geometry, the  $\epsilon_r$  of these semiconducting polymers was accurately determined by frequency-scan BDS at various temperatures. Indeed, the  $\epsilon_r$  values of P1, P2, and P3 increased from 3.75 for P3HT to 7.4, 9.3, and 8.1, respectively, at 1 MHz and room temperature. To the best of our knowledge, these are among the highest  $\epsilon_r$  values based on reliable measurements reported for conjugated polymers. At this moment, we speculate that both sulfinyl/sulfonyl groups in the amorphous phase and in the crystals contribute to the high dielectric constant of P1–P3.

Although the P3HT crystalline structure and the conjugation length were largely preserved for the side-chain-functionalized P1–P3, the highly interacting sulfinyl and sulfonyl groups may facilitate vibrational relaxation of the polythiophene backbones, resulting in weakened vibronic absorption bands in UV–vis and decreased fluorescence intensity for thin films. In particular, P2 largely lost the vibronic bands, and fluorescence was quenched in the solid state. This was attributed to the slight oxidation of the polythiophene units in the main chain of P2. In this sense, P1 with sulfinyl groups had a lower impact on optical properties in thin films than P2 with sulfonyl groups, suggesting that methylsulfinyl end groups may provide a balance between obtaining high  $\epsilon_r$  and preserving favorable  $\pi$ – $\pi$  interaction for the polythiophene backbones. Research is currently underway to explore the charge transport properties (i.e., charge concentration and mobility) of P1–P3 using combined

broadband dielectric spectroscopy and computer simulation, and device performance will be reported in the future.

## ACKNOWLEDGMENTS

We are grateful to the National Science Foundation (NSF, CHEM-1148652) for funding this project. BDS characterization by Z.Z. and L.Z. is supported by NSF, Division of Materials Research (DMR), Polymers Program (DMR-1708990). We thank Dr. Forrest Etheridge for advice on synthesis, Dr. Eric Baer for DSC measurement, Dr. James Burgess for facilitating cyclic voltammetry, and Dr. Emily Pentzer for providing access to UV-vis instrument. The MALDI-TOF instrument was supported by NSF under Grant MRI-0821515. GI-WAXD experiments were performed at the 11-BM CMS beamline of NSLS-II, BNL, a U.S. Department of Energy User Facility operated for the Office of Science by BNL under Contract DESC0012704.

## REFERENCES

- (1) Miyata, A.; Mitioglu, A.; Plochocka, P.; Portugall, O.; Wang, J. T. W.; Stranks, S. D.; Snaith, H. J.; Nicholas, R. J. Direct Measurement of the Exciton Binding Energy and Effective Masses for Charge Carriers in Organic-Inorganic Tri-Halide Perovskites. *Nat. Phys.* **2015**, *11*, 582–587.
- (2) Kraner, S.; Scholz, R.; Koerner, C.; Leo, K. Design Proposals for Organic Materials Exhibiting a Low Exciton Binding Energy. *J. Phys. Chem. C* **2015**, *119*, 22820–22825.
- (3) Green, M. A.; Ho-Baillie, A.; Snaith, H. J. The Emergence of Perovskite Solar Cells. *Nat. Photonics* **2014**, *8*, 506–514.
- (4) Poglitsch, A.; Weber, D. Dynamic Disorder in Methylammoniumtrihalogenoplumbates (II) Observed by Millimeter-Wave Spectroscopy. *J. Chem. Phys.* **1987**, *87*, 6373–6378.
- (5) Miyata, K.; Meggiolaro, D.; Trinh, M. T.; Joshi, P. P.; Mosconi, E.; Jones, S. C.; De Angelis, F.; Zhu, X. Y. Large Polarons in Lead Halide Perovskites. *Sci. Adv.* **2017**, *3*, e1701217.

- (6) Frost, J. M.; Butler, K. T.; Brivio, F.; Hendon, C. H.; van Schilfgaarde, M.; Walsh, A. Atomistic Origins of High-Performance in Hybrid Halide Perovskite Solar Cells. *Nano Lett.* **2014**, *14*, 2584–2590.
- (7) Nayak, P. K. Exciton Binding Energy in Small Organic Conjugated Molecule. *Synth. Met.* **2013**, *174*, 42–45.
- (8) Dkhissi, A. Excitons in Organic Semiconductors. *Synth. Met.* **2011**, *161*, 1441–1443.
- (9) Hummer, K.; Ambrosch-Draxl, C. Oligoacene Exciton Binding Energies: Their Dependence on Molecular Size. *Phys. Rev. B: Condens. Matter Mater. Phys.* **2005**, *71*, No. 081202, DOI: 10.1103/PhysRevB.71.081202.
- (10) van der Horst, J. W.; Bobbert, P. A.; Michels, M. A. J.; Bassler, H. Calculation of Excitonic Properties of Conjugated Polymers Using the Bethe-Salpeter Equation. *J. Chem. Phys.* **2001**, *114*, 6950–6957.
- (11) Zhang, G.; Clarke, T. M.; Mozer, A. J. Bimolecular Recombination in a Low Bandgap Polymer:PCBM Blend Solar Cell with a High Dielectric Constant. *J. Phys. Chem. C* **2016**, *120*, 7033–7043.
- (12) Koster, L. J. A.; Shaheen, S. E.; Hummelen, J. C. Pathways to a New Efficiency Regime for Organic Solar Cells. *Adv. Energy Mater.* **2012**, *2*, 1246–1253.
- (13) Torabi, S.; Jahani, F.; Van Severen, I.; Kanimozhi, C.; Patil, S.; Havenith, R. W. A.; Chiechi, R. C.; Lutsen, L.; Vanderzande, D. J. M.; Cleij, T. J.; Hummelen, J. C.; Koster, L. J. A. Strategy for Enhancing the Dielectric Constant of Organic Semiconductors Without Sacrificing Charge Carrier Mobility and Solubility. *Adv. Funct. Mater.* **2015**, *25*, 150–157.
- (14) Brebels, J.; Manca, J. V.; Lutsen, L.; Vanderzande, D.; Maes, W. High Dielectric Constant Conjugated Materials for Organic Photovoltaics. *J. Mater. Chem. A* **2017**, *5*, 24037–24050.
- (15) Zhu, L. Exploring Strategies for High Dielectric Constant and Low Loss Polymer Dielectrics. *J. Phys. Chem. Lett.* **2014**, *5*, 3677–3687.
- (16) Kremer, F.; Schönhals, A. *Broadband Dielectric Spectroscopy*; Springer: Berlin, 2003.
- (17) Baer, E.; Zhu, L. 50th Anniversary Perspective: Dielectric Phenomena in Polymers and Multilayered Dielectric Films. *Macromolecules* **2017**, *50*, 2239–2256.
- (18) Wang, C. C.; Pilania, G.; Boggs, S. A.; Kumar, S.; Breneman, C.; Ramprasad, R. Computational Strategies for Polymer Dielectrics Design. *Polymer* **2014**, *55*, 979–988.
- (19) Zhao, Z.; Zhang, Z.; Pejic, S.; Zhang, G.; Zhu, Y.; Liu, H.; Litt, M.; Sauve, G.; Zhu, L. Synergistic Dielectric and Semiconducting Properties in Fluorescein Monopotassium Salt Random Copolymers. *Polymer* **2017**, *114*, 189–198.
- (20) Leblebici, S.; Lee, J.; Weber-Bargioni, A.; Ma, B. W. Dielectric Screening To Reduce Charge Transfer State Binding Energy in Organic Bulk Heterojunction Photovoltaics. *J. Phys. Chem. C* **2017**, *121*, 3279–3285.
- (21) de Gier, H. D.; Broer, R. Non-Innocent Side-Chains with Dipole Moments in Organic Solar Cells Improve Charge Separation. *Phys. Chem. Chem. Phys.* **2014**, *16*, 12454–12461.
- (22) Yang, P.; Yuan, M.; Zeigler, D. F.; Watkins, S. E.; Lee, J. A.; Luscombe, C. K. Influence of Fluorine Substituents on the Film Dielectric Constant and Open-Circuit Voltage in Organic Photovoltaics. *J. Mater. Chem. C* **2014**, *2*, 3278–3284.
- (23) Cho, N.; Schlenker, C. W.; Knesting, K. M.; Koelsch, P.; Yip, H. L.; Ginger, D. S.; Jen, A. K. Y. High-Dielectric Constant Side-Chain Polymers Show Reduced Non-Geminate Recombination in Heterojunction Solar Cells. *Adv. Energy Mater.* **2014**, *4*, 1301857.
- (24) Armin, A.; Stoltzfus, D. M.; Donaghey, J. E.; Clulow, A. J.; Nagiri, R. C. R.; Burn, P. L.; Gentle, I. R.; Meredith, P. Engineering Dielectric Constants in Organic Semiconductors. *J. Mater. Chem. C* **2017**, *5*, 3736–3747.
- (25) Kao, K.-C. *Dielectric Phenomena in Solids: With Emphasis on Physical Concepts of Electronic Processes*; Elsevier Academic Press: Boston, MA, 2004.

- (26) Wei, J.; Zhang, Z.; Tseng, J.-K.; Treufeld, I.; Liu, X.; Litt, M. H.; Zhu, L. Achieving High Dielectric Constant and Low Loss Property in a Dipolar Glass Polymer Containing Strongly Dipolar and Small-Sized Sulfone Groups. *ACS Appl. Mater. Interfaces* **2015**, *7*, 5248–5257.
- (27) Zhang, Z.; Wang, D. H.; Litt, M. H.; Tan, L.-S.; Zhu, L. High-Temperature and High-Energy-Density Dipolar Glass Polymers Based on Sulfonated Poly(2,6-dimethyl-1,4-phenylene oxide). *Angew. Chem., Int. Ed.* **2018**, *57*, 1528–1531.
- (28) Zhu, Y.-F.; Zhang, Z.; Litt, M. H.; Zhu, L. High Dielectric Constant Sulfonyl-Containing Dipolar Glass Polymers with Enhanced Orientational Polarization. *Macromolecules* **2018**, *51*, 6257.
- (29) Zhai, L.; Pilston, R. L.; Zaiger, K. L.; Stokes, K. K.; McCullough, R. D. A Simple Method to Generate Side-Chain Derivatives of Regioregular Polythiophene via the GRIM Metathesis and Post-Polymerization Functionalization. *Macromolecules* **2003**, *36*, 61–64.
- (30) Armarego, W. L. F.; Chai, C. L. L. *Purification of Laboratory Chemicals*, 7th ed.; Elsevier/Butterworth-Heinemann: Amsterdam, 2013.
- (31) Iovu, M. C.; Sheina, E. E.; Gil, R. R.; McCullough, R. D. Experimental Evidence for the Quasi-“Living” Nature of the Grignard Metathesis Method for the Synthesis of Regioregular Poly(3-alkylthiophenes). *Macromolecules* **2005**, *38*, 8649–8656.
- (32) Loewe, R. S.; Khersonsky, S. M.; McCullough, R. D. A Simple Method to Prepare Head-to-Tail Coupled, Regioregular Poly(3-alkylthiophenes) Using Grignard Metathesis. *Adv. Mater.* **1999**, *11*, 250–253.
- (33) Lanzi, M.; Paganin, L. New Regioregular Polythiophenes Functionalized with Sulfur-Containing Substituents for Bulk Heterojunction Solar Cells. *React. Funct. Polym.* **2010**, *70*, 346–360.
- (34) Rodrigues, A.; Castro, M. C. R.; Farinha, A. S. F.; Oliveira, M.; Tome, J. P. C.; Machado, A. V.; Raposo, M. M. M.; Hilliou, L.; Bernardo, G. Thermal Stability of P3HT and P3HT:PCBM Blends in the Molten State. *Polym. Test.* **2013**, *32*, 1192–1201.
- (35) Snyder, C. R.; Nieuwendaal, R. C.; DeLongchamp, D. M.; Luscombe, C. K.; Sista, P.; Boyd, S. D. Quantifying Crystallinity in High Molar Mass Poly(3-hexylthiophene). *Macromolecules* **2014**, *47*, 3942–3950.
- (36) Shao, M.; Keum, J.; Chen, J.; He, Y.; Chen, W.; Browning, J. F.; Jakowski, J.; Sumpster, B. G.; Ivanov, I. N.; Ma, Y.; Rouleau, C. M.; Smith, S. C.; Geohegan, D. B.; Hong, K.; Xiao, K. The Isotopic Effects of Deuteration on Optoelectronic Properties of Conducting Polymers. *Nat. Commun.* **2014**, *5*, 3180.
- (37) Alemseghed, M. G.; Gowrisanker, S.; Servello, J.; Stefan, M. C. Synthesis of Di-Block Copolymers Containing Regioregular Poly(3-hexylthiophene) and Poly(tetrahydrofuran) by a Combination of Grignard Metathesis and Cationic Polymerizations. *Macromol. Chem. Phys.* **2009**, *210*, 2007–2014.
- (38) Alemseghed, M. G.; Servello, J.; Hundt, N.; Sista, P.; Biewer, M. C.; Stefan, M. C. Amphiphilic Block Copolymers Containing Regioregular Poly(3-hexylthiophene) and Poly(2-ethyl-2-oxazoline). *Macromol. Chem. Phys.* **2010**, *211*, 1291–1297.
- (39) Li, W.; He, Y.-G.; Shi, S.-Y.; Liu, N.; Zhu, Y.-Y.; Ding, Y.-S.; Yin, J.; Wu, Z.-Q. Fabrication of a Multi-Charge Generable Poly(phenyl isocyanide)-Block-Poly(3-hexylthiophene) Rod-Rod Conjugated Copolymer. *Polym. Chem.* **2015**, *6*, 2348–2355.
- (40) Liu, N.; Qi, C.-G.; Wang, Y.; Liu, D.-F.; Yin, J.; Zhu, Y.-Y.; Wu, Z.-Q. Solvent-Induced White-Light Emission of Amphiphilic Rod-Rod Poly(3-triethylene glycol thiophene)-Block-Poly(phenyl isocyanide) Copolymer. *Macromolecules* **2013**, *46*, 7753–7758.
- (41) Wei, S. J.; Xia, J. L.; Dell, E. J.; Jiang, Y. V.; Song, R.; Lee, H.; Rodenbough, P.; Briseno, A. L.; Campos, L. M. Bandgap Engineering through Controlled Oxidation of Polythiophenes. *Angew. Chem., Int. Ed.* **2014**, *53*, 1832–1836.
- (42) Barbarella, G.; Pudova, O.; Arbizzani, C.; Mastragostino, M.; Bongini, A. Oligothiophene-S,S-Dioxides: a New Class of Thiophene-Based Materials. *J. Org. Chem.* **1998**, *63*, 1742–1745.
- (43) Tsai, C.-H.; Chirdon, D. N.; Maurer, A. B.; Bernhard, S.; Noonan, K. J. T. Synthesis of Thiophene 1,1-Dioxides and Tuning Their Optoelectronic Properties. *Org. Lett.* **2013**, *15*, 5230–5233.
- (44) Mao, Z.; Vakhshouri, K.; Jaye, C.; Fischer, D. A.; Fernando, R.; DeLongchamp, D. M.; Gomez, E. D.; Sauve, G. Synthesis of Perfluoroalkyl End-Functionalized Poly(3-hexylthiophene) and the Effect of Fluorinated End Groups on Solar Cell Performance. *Macromolecules* **2013**, *46*, 103–112.
- (45) Cui, J.; Martinez-Tong, D. E.; Sanz, A.; Ezquerro, T. A.; Rebollar, E.; Nogales, A. Relaxation and Conductivity in P3HT/PC71BM Blends as Revealed by Dielectric Spectroscopy. *Macromolecules* **2016**, *49*, 2709–2717.
- (46) Huang, H.; Chen, X.; Yin, K.; Treufeld, I.; Schuele, D. E.; Ponting, M.; Langhe, D.; Baer, E.; Zhu, L. Reduction of Ionic Conduction Loss in Multilayer Dielectric Films by Immobilizing Impurity Ions in High Glass Transition Temperature Polymer Layers. *ACS Appl. Energy Mater.* **2018**, *1*, 775–782.
- (47) Li, J. V.; Nardes, A. M.; Liang, Z.; Shaheen, S. E.; Gregg, B. A.; Levi, D. H. Simultaneous Measurement of Carrier Density and Mobility of Organic Semiconductors Using Capacitance Techniques. *Org. Electron.* **2011**, *12*, 1879–1885.
- (48) Mackey, M.; Schuele, D. E.; Zhu, L.; Baer, E. Layer Confinement Effect on Charge Migration in Polycarbonate/Poly(vinylidene fluorid-co-hexafluoropropylene) Multilayered Films. *J. Appl. Phys.* **2012**, *111*, 113702.
- (49) Yang, L.; Allahyarov, E.; Guan, F.; Zhu, L. Crystal Orientation and Temperature Effects on Double Hysteresis Loop Behavior in a Poly(vinylidene fluoride-co-trifluoroethylene-co-chlorotrifluoroethylene)-Graft-Polystyrene Graft Copolymer. *Macromolecules* **2013**, *46*, 9698–9711.
- (50) Mozer, A. J.; Sariciftci, N. S.; Pivrikas, A.; Osterbacka, R.; Juska, G.; Brassat, L.; Bassler, H. Charge carrier mobility in regioregular poly(3-hexylthiophene) probed by transient conductivity techniques: A comparative study. *Phys. Rev. B: Condens. Matter Mater. Phys.* **2005**, *71*, No. 035214, DOI: 10.1103/PhysRevB.71.035214.
- (51) Lu, G.; Blakesley, J.; Himmelberger, S.; Pingel, P.; Frisch, J.; Lieberwirth, I.; Salzmann, I.; Oehzelt, M.; Di Pietro, R.; Salleo, A.; Koch, N.; Neher, D. Moderate Doping Leads to High Performance of Semiconductor/Insulator Polymer Blend Transistors. *Nat. Commun.* **2013**, *4*, 1588.
- (52) Balendhran, S.; Deng, J.; Ou, J. Z.; Walia, S.; Scott, J.; Tang, J.; Wang, K. L.; Field, M. R.; Russo, S.; Zhuiykov, S.; Strano, M. S.; Medhekar, N.; Sriram, S.; Bhaskaran, M.; Kalantar-Zadeh, K. Enhanced Charge Carrier Mobility in Two-Dimensional High Dielectric Molybdenum Oxide. *Adv. Mater.* **2013**, *25*, 109–114.